2014

In Actu Et In Silicio: Linear and Nonlinear Photophysical Characterization of a Novel Europium Complex, and Incorporating Computational Calculations in the Analysis of Novel Organic Compounds

Adam Woodward
University of Central Florida

IN ACTU ET IN SILICIO: LINEAR AND NONLINEAR PHOTOPHYSICAL CHARACTERIZATION OF A NOVEL EUROPIUM COMPLEX, AND INCORPORATING COMPUTATIONAL CALCULATIONS IN THE ANALYSIS OF NOVEL ORGANIC COMPOUNDS

by

ADAM WOODWARD
MChem University of East Anglia, 2009

A dissertation submitted in partial fulfillment of the requirements
for the degree of Doctor of Philosophy
in the Department of Chemistry
in the College of Sciences
at the University of Central Florida
Orlando, Florida

Fall Term
2014

Major Professor: Kevin D. Belfield

ABSTRACT

Despite not being a tangible substance, light is becoming an increasingly valuable tool in numerous areas of science and technology: the use of laser excitation of a fluorescent probe can generate incredibly detailed images of cellular structures without the need for large amounts of dissection; new types of solar cells are being produced using organic dyes to harvest light; computer data can be stored by inducing a chemical change in a compound through irradiation with light. However, before any of these materials can be applied in such a way, their properties must first be analyzed for them to be deemed viable.

The focus of this dissertation is the photophysical characterization, linear and nonlinear, of a several novel organic compounds, and a europium complex, as well as using quantum chemical calculation techniques to understand some of the phenomena that are witnessed and begin to develop predictive capability. The nonlinear characterization of compounds utilizes wavelengths outside of their linear absorption range, where a focused beam can achieve the same excitation as one at half the wavelength, though this effect has a quadratic dependence on power.

The potential for nonlinear excitation, or two-photon absorption (2PA), is becoming of increasing interest and importance for organic chromophores. Exciting only a small

volume of material at a focal point makes it possible to nondestructively image samples in 3-dimensions, record data in multiple layers, and fabricate intricate structures through photopolymerization reactions.

Lanthanides such as europium are known to exhibit sharp emission bands when excited, typically through an antenna effect due to the low probability of achieving direct excitation. This emission is long-lived, and through gating systems can readily be separated from background noise and autofluorescence (often observed in biological samples) that have much shorter lifetimes. Thus, one of the foci of this dissertation is the photophysical investigation of a series of novel lanthanide complexes, with particular attention to a europium complex.

For my Granddad Jim

ACKNOWLEDGMENTS

My supervisor, Dr. Kevin D. Belfield, has been a great leader to our research group, and I am grateful for advice and support that he has given to not only to me and my research, but also to the other students within the group, both under and postgraduate.

I would like to thank Dr. Mykhailo V. Bondar for his intellectual guidance, constructive criticisms, and always being available and willing to answer a question. Also, an appreciation to Drs. Alma R. Morales and Andrew Frazer for their suggestions and support from when I first joined the group up to the current day.

My thanks also go to Dr. James Harper, who got me started with DFT calculations; and to Dr. Artem Masunov for being able to guide my efforts beyond the cliff of my initial training.

Of course none of the work in this dissertation would have been possible, were it not for the synthetic skills of Dr. Frazer, Grace Githaiga, and Ebrahim Ghazvini Zadeh. In addition to these, Dr. William Moreshead, Dr. Morales, Alfonso Ballestas Barrientos, Hafeez Haniff, Fengchun Li have all kept me busy with the work on compounds they synthesized. There have also been valuable discussions with Bosung Kim and Simon Tang, as well as the other members of the Belfield research group present during our meetings.

I also appreciate the support I have received from friends and family, on both sides of the Atlantic.

TABLE OF CONTENTS

LIST OF FIGURES

LIST OF TABLES

LIST OF ABBREVIATIONS

2PA	Two-photon absorption
Å	Angstrom (10^{-10} meters)
Abs	Absorption
BODIPY	Boron-dipyrromethene
c	Concentration
CHX	Cyclohexane
cm	Centimeter
CW	Continuous wave
D	Debye
DCB	1,2-dichlorobenzene
DCM	Dichloromethane
DFT	Density functional theory
dm	Decimeter
DPA	9,10-diphenylanthracene
e	Mathematical constant, 2.718
Em	Emission

Ex	Excitation
fs	Femtosecond
FWHM	Full width, half maximum
g	Gerade (German for even)
GM	Göppert-Meyers (10^{-50} cm^{-4}photons s^{-1})
Hex	Hexane
HOMO	Highest occupied molecular orbital
I	Fluorescence intensity
I_0	Initial intensity
I_t	Intensity at time t
I_z	Intensity at position z
IC	Internal conversion
ISC	Intersystem crossing
kHz	Kilohertz (10^3 hertz)
LUMO	Lowest unoccupied molecular orbital
MHz	Megahertz (10^6 hertz)

mm	Millimeter (10^{-3} meters)
ms	Millisecond (10^{-3} seconds)
mol	Moles
mW	Milliwatts (10^{-3} watts)
n	Refractive index
NIR	Near infrared
nm	Nanometer (10^{-9} meters)
ns	Nanosecond (10^{-9} seconds)
NA	Number of photons absorbed
OD	Optical density
pTHF	Polytetrahydrofuran
R	Anisotropy
s	Second
S_0	Singlet ground state
S_1	First excited singlet state
t	Time
T_1	First excited triplet state

TD-DFT	Time dependent density functional theory
TEA	Triethylamine
TFA	Trifluoroacetic acid
THF	Tetrahydrofuran
Tol	Toluene
u	Ungerade (German for uneven)
z	Position along the path of a laser beam

δ_{2PA}	Maximum 2PA cross section
ε	Extinction coefficient
ϵ	Dielectric constant
λ	Wavelength
μm	Micrometer (10^{-6} meters)
μs	Microsecond (10^{-6} seconds)
σ_n	N-photon cross section
τ_f	Fluorescence lifetime

τ_l	Luminescence lifetime
φ	Dihedral angle
Φ_f	Fluorescence quantum yield
Φ_l	Luminescence quantum yield
Φ_{Ph}	Photodecomposition quantum yield

I – INTRODUCTION

"I am almost inclined to coin a word, and call the appearance fluorescence, from fluor-spar, as the analogous term opalescence is derived from the name of a mineral."[1]

Sir George Stokes (1819 – 1903)

Linear spectroscopy: absorption and fluorescence

All ordinary matter absorbs electromagnetic radiation.[2] How much of that radiation and how it is utilized is dependent on the absorbing chemical and on the wavelength of radiation. High energy electromagnetic radiation (Figure 1), in the form of X-rays and ultraviolet light is capable of breaking the bonds between atoms,[3, 4] while at lower energies, microwaves and infrared radiation will only rotate[5] or cause bond vibrations within a molecule,[6] respectively. Between these regions lies the small domain that is observable to the naked eye: visible light.

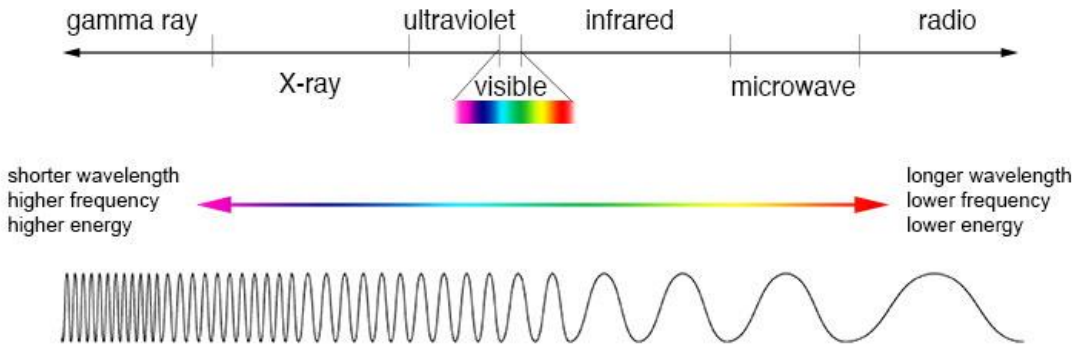

Figure 1: The electromagnetic spectrum. [Reproduced with permission from reference [7], copyright NASA's Imagine the Universe.]

Absorption of these visible wavelengths can provide a molecule with sufficient energy to be promoted to an excited electronic singlet state; this is particularly prevalent in organic compounds with conjugated π-systems. Once this excited state is achieved, the additional energy is dissipated in one of several ways, depending on the molecule and the system it is in: emission of a photon through fluorescence or phosphorescence (preceded by intersystem crossing to a triplet state), radiationless internal conversion back to the ground state, or transfer to another species in close proximity. These processes can be illustrated in a Jablonski diagram (Figure 2).

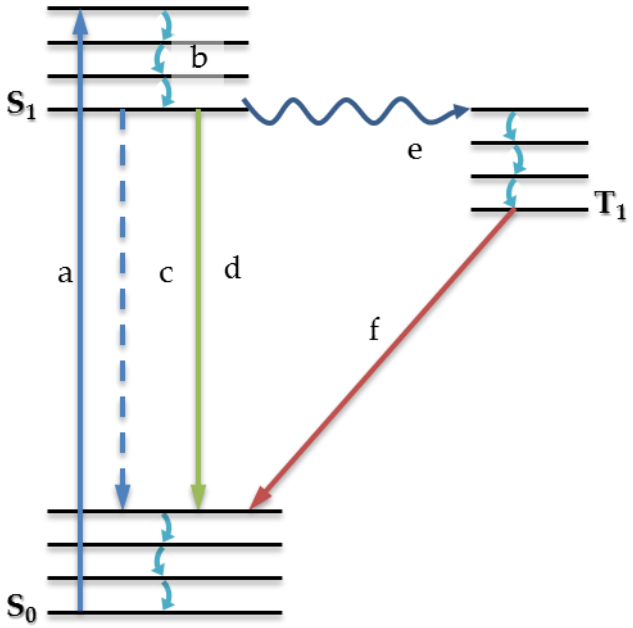

Figure 2: A Jablonski diagram showing the possible routes of a species after the absorption of light, and being promoted to an excited singlet state (a): vibrational relaxation (b), internal conversion (c), fluorescence (d), intersystem crossing (e), and phosphorescence (f).

While atomic fluorescence is observed at the same wavelength as its excitation, molecular fluorescence is recorded at longer wavelengths. This is in part due to the loss of energy through vibrational relaxation to reach an emissive state, as well as the rearrangement of solvent molecules surrounding the fluorophore to stabilize the change in the dipole that accompanies the excitation. In the case of non-polar solvents, such as hexane or toluene, little energy is expended, and so the shift is nominal;[8] for polar species, including dichloromethane (DCM) and tetrahydrofuran (THF), the solvent molecules are

more effective at stabilizing the excited state of the fluorophore, lowering it in energy, resulting in a bathochromically shifted emission (Figure 3).[9] This is effect of solvent polarity is known as solvatochromism,[10] and the difference between the maxima wavelengths of absorption and emission is termed the Stokes shift, in reference to the man who gave a detailed account of the phenomenon: Sir George Stokes.[1, 9]

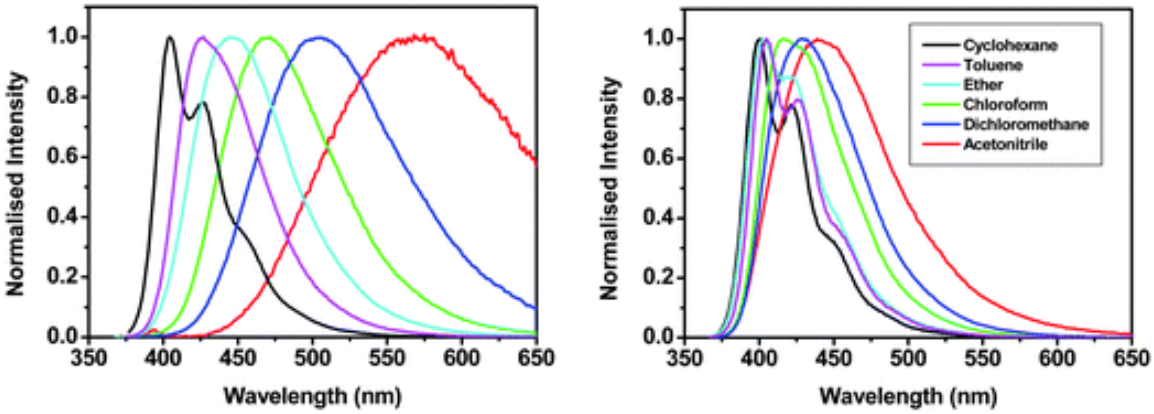

Figure 3: Solvatochromic shifts seen for two carbazole diaryloxadiazole hybrid compounds across a range of solvent polarities. [Reproduced from reference [8] with permission from The Royal Society of Chemistry.]

Fluorescence emission is not a flawless process however: solvatochromic effects can result in a decrease in fluorescence intensity, and the intrinsic emissive properties of one compound can be noticeably different to those of another. As such, fluorescence quantum yields are measured for fluorophores:

the ratio between the number of photons emitted and the number absorbed. This value is usually measured in one of two ways – directly, using an integrating sphere to collect all of the emitted light,[11] or relative to a reference compound.[9] This latter method requires the use of Equation 1, where Φ is the fluorescence quantum yield, *OD* is the optical density at the excitation wavelength, *I* is the integrated fluorescence intensity, *n* is the refractive index of the solvent.[9]

$$\Phi_f = \Phi_{ref}\left(\frac{OD_{ref}}{OD}\right)\left(\frac{\int I}{\int I_{ref}}\right)\left(\frac{n^2}{n_{ref}^2}\right) \quad \textbf{(1)}$$

Irradiating with a continuous wave (CW) light source, the emission of a fluorophore appears constant. However with the use of a pulsed excitation source, it is possible to record a time-resolved decay trace, from which a lifetime, τ, of the luminescent signal can be calculated (Equation 2).[12]

$$I_t = I_0 e^{-t/\tau} \quad \textbf{(2)}$$

In the case of fluorescence, this lifetime falls in the range of 10^{-12} – 10^{-6} s, while phosphorescence can last significantly longer, 10^{-3} – 10^{2} s, due to the formally

forbidden nature of the transition.[13] The rate of this decay is also affected by solvatochromism, in that high polarity solvents will result in a shorter lifetime of the luminescence.[9]

It is possible to probe the excitation spectrum of a compound to determine the presence of a single transition within an absorption band (typically the main). This can be achieved using polarized excitation light, as it will generally lead to the emission of polarized emission if the excited state lifetime is less than the molecule's rotational reorientation (diffusion) time. The anisotropy is probed by determining the emission, parallel versus orthogonal to the excitation light. The measurement of excitation anisotropy, that is the excitation spectra collected for a polarized emission upon excitation with polarized light, is typically done in viscous solvents (such as polytetrahydrofuran (pTHF) or glycerol) so that the rotation time of the molecule is much longer than the lifetime of the excited state (Figure 4). If a plateau is evident within an absorption band, it indicates the presence of a single transition.[14] Points of inflection in an anisotropy trace can be used as a guide to where nonlinear transitions may be present, given the overlap of transitions at that wavelength.

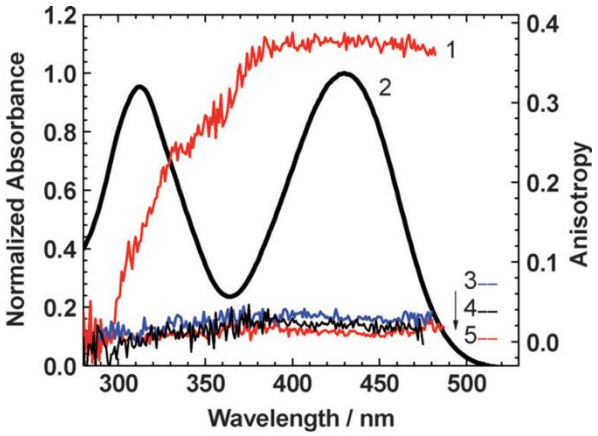

Figure 4: Example of anisotropy spectra for a diphenylaminofluorene thionylchalcone in pTHF (1), THF (3), toluene (4), and hexane (5) plotted against the linear absorption spectrum in THF (2). [Reproduced with permission from reference [14], copyright 2012 WILEY-VCH Verlag GmbH & Co.]

Through continual irradiation, chromophore systems can become damaged or bleached. As this would affect their viability, it becomes necessary to measure a compound's photostability. The photodecomposition quantum yield is a quantity used to determine photostability. Changes in concentration of the species of interest, determined by collecting absorption spectra collected over a period of time are combined with the energy of the irradiation source and used to determine the photodecomposition quantum yield (Φ_{Ph}) through Equation 3, where $D(\lambda, 0)$, $D(\lambda,t_{ir})$ are the initial and final optical density of the solution, $\varepsilon(\lambda)$ is the extinction coefficient ($dm^3\ mol^{-1}\ cm^{-1}$), t is irradiation time (s) and λ is excitation wavelength (cm), N_A is Avogadro's number, t_{ir} is total irradiation time, $I_0(\lambda)$ is the spectral distribution of the excitation irradiance.[15]

$$\Phi_{Ph} = \frac{[D(\lambda, 0) - D(\lambda, t_{ir})]N_A}{10^3 \varepsilon(\lambda) \int_{\lambda} \int_0^{t_{ir}} I_0(\lambda)\,[1 - 10^{D(\lambda,t)}]\,d\lambda\,dt} \quad (3)$$

Nonlinear spectroscopy: two-photon absorption

In her 1930 doctoral thesis, Maria Göppert-Mayer predicted the ability for a molecule to absorbed two photons simultaneously,[16] though the concept was not proven until the advent of laser technology in the 1960s.[17] From the molecular viewpoint, the two absorbed photons have the same effect as one with the sum frequency of the two (Figure 5). However, in order for excitation to be achieved, the photons must be absorbed within a short space of time, in the femtosecond (fs) time domain; otherwise the energy is simply dissipated.

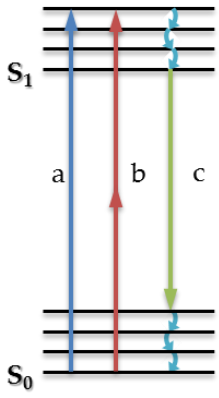

Figure 5: A Jablonski diagram comparing one-photon (a) and two-photon (b) excitation of fluorescence (c).

In the case of single photon absorption, the Beer-Lambert law (Equation 4), where I_0 and I are the intensities of light initially and after the sample, respectively, ε is the extinction coefficient for the sample (given in $dm^3\ mol^{-1}\ cm^{-1}$), c is the concentration of the sample (in mol dm^{-3}), and l is the path length of the sample (in cm), explains change of intensity of an incident beam as it passes through a sample. At the molecular level, a cross sectional area can be defined for a chromophore over which it absorbs the incident light and this absorption is proportional to the intensity of the light (Equation 5, where NA is the number of photons absorbed per second (photon s^{-1}) and σ_1 is the one-photon cross section of the molecule (cm^2)).[9]

$$\boldsymbol{I = I_0 e^{-\varepsilon c l}} \quad \textbf{(4)}$$

$$\boldsymbol{NA = \sigma_1 \cdot I_0} \quad \textbf{(5)}$$

Moving to two-photon absorption, excitation requires quick successive absorption of the photons by a single molecule. This is most achievable in the focal point of a beam, where $z = z_0 = 0$. Equation 6 indicates that the transmission intensity at a specific z position is affected by the product of the two-photon absorption cross section, σ_2, and the excitation intensity squared, due to the

involvement of the two separate photons. Integration of Equation 6 with respect to *z* yields the equation for two-photon absorption, Equation 7.[18]

$$\frac{\partial I}{\partial z} = -NA \cdot \sigma_2 \cdot I_0^2 \quad \textbf{(6)}$$

$$I_Z = I_{Z_0} \frac{1}{1 + \sigma_2 \cdot NA \cdot I_{Z_0} \cdot z} \quad \textbf{(7)}$$

From Equation 6, it can also be noted the quadratic dependency on the incident irradiation, making this a nonlinear technique. Typical values calculated for two-photon absorption (2PA) cross sections are in range of 10^{-48}-10^{-50} cm^4 s $photon^{-1}$, but this is simplified to the units GM, named for Göppert-Mayer, where 1 GM = 10^{-50} cm^4 s $photon^{-1}$.

The localized excitation gives rise to only an isolated fluorescence signal (Figure 6). This facilitates effective 3-dimensional techniques, such as microfabrication,[19] optical data storage,[20] and fluorescence microscopy.[21] In such cases, limiting the excitation to the focal point within the sample prevents any out of focus fluorescence, which can lead to bleaching of the fluorophore.

Figure 6: Photograph illustrating the localized fluorescence from fluorescein achieved when exciting through two-photon (760 nm, right) compared to one (380 nm, left). [Reproduced from reference [22], copyright 2014 Belfield Research Group at the University of Central Florida]

In the case of two-photon fluorescence microscopy of biological samples, there are additional advantages: nonlinear excitation limits the bleaching of the dyes being used, as well as preventing damage to the cells outside of the focal plane. Also, two-photon excitation wavelengths typically fall into the red or near-infrared (NIR) region of the spectrum. At these wavelengths, the innate absorption of biological species, such as hemoglobin and oxyhemoglobin, and water are relatively low (Figure 7), increasing the penetration depths that can be achieved, evidenced by the 1.6 mm image in Figure 8.

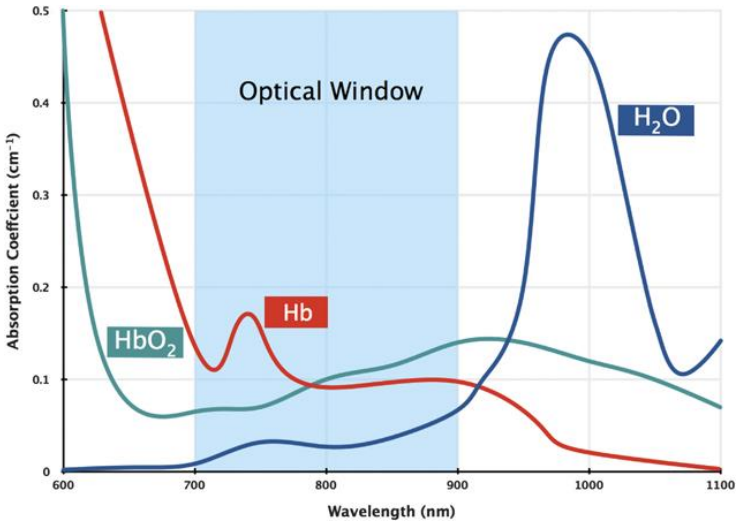

Figure 7: Absorption spectra for hemoglobin, oxyhemoglobin, and water illustrating the optical window between 700 –900 nm. [Reproduced with permission from reference [23], copyright 2012 Nature Publishing Group]

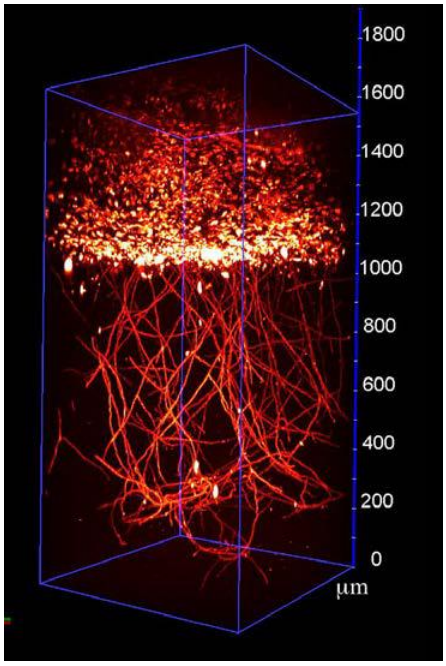

Figure 8: Reconstructed 3-dimensional image of the vasculature formed in a wound healing model, achieved through stacking 1600 1 µm 2-dimensional images. [Reproduced from reference [21].]

For a compound to be a suitable candidate for applications such as two-photon fluorescence bioimaging, it should exhibit a high fluorescence quantum yield and high 2PA cross section, while having high photostability, or low photodecomposition quantum yield. To evaluate these properties, a figure of merit, F_M, is used to give a direct value for comparing prospective compounds, calculated as per Equation 8, where Φ_f is the fluorescence quantum yield, δ is the maximum 2PA cross section, and Φ_{Ph} is the photodecomposition quantum yield.[24, 25]

$$F_M = \frac{\Phi_f \delta_{2PA}}{\Phi_{Ph}} \quad (8)$$

Interest in the development of novel two-photon absorbing dyes for a variety of purposes is an increasingly prevalent area of research. This work investigates several such compounds, probing their linear and nonlinear properties, as well as performing quantum chemical calculations to provide a more in-depth understanding of the results.

II: PROBING A PURE COLOR – PHOTOPHYSICAL CHARACTERIZATION OF A EUROPIUM COMPLEX

Two-photon sensitized visible and near-IR luminescence of lanthanide complexes using a fluorene-based donor–π-acceptor diketonate

A. W. Woodward, A. Frazer, A. R. Morales, J. Yu, A. F. Moore, A. D. Campiglia, E. V. Jucov, T. V. Timofeeva and K. D. Belfield, *Dalton Trans.*, 2014, **43**, 16626-16639, DOI**:** 10.1039/C4DT01507J - Reproduced by permission of The Royal Society of Chemistry

Abstract

A fluorene-based donor-acceptor ligand was successfully employed to sensitize visible and near-IR emitting lanthanide centers. Detailed characterization of these complexes was conducted, with particular emphasis on linear and nonlinear photophysical properties. Steady-state and time-resolved emission spectroscopy and overall luminescence quantum yield measurements were performed on all the complexes. In addition, excitation anisotropy and two-photon absorption spectra (via z-scan) were obtained for the ligand and europium complex, revealing a maximum 2PA cross section of 340 GM for the

latter upon excitation at 760 nm. A quadratic relationship was found by varying laser excitation power versus luminescence intensity of the europium complex, confirming sensitization via two-photon excitation.

Introduction

Lanthanides possess optical properties that make them ideally suited for use in biomedical microscopy techniques, such as fluorescence bioimaging; the long lifetime of their luminescence emission allows facile separation of signal from residual noise.[26-28] Their sharp, narrow emission profiles also make them attractive for material applications, such as use in lasers and light emitting diodes.[29, 30]

These unique properties of lanthanide elements are offset by the ability to access them; direct excitation of a lanthanide is inherently difficult due to the low absorption coefficients of the Laporte forbidden f-f transitions that are responsible for the emission. Instead, excitation is achieved via a proxy: a ligated antenna chromophore is employed for which direct excitation is easily achieved, and the energy is transferred via a triplet state.[31] The use of β-diketonate ligands is popular due to the commercial availability of a variety of different ligands, and

the facile nature of complexing the ligand to the metal center.[29, 32, 33] However, once dissolved, β-diketonate complexes undergo rapid interchange of ligands, leading to a plethora of species in solution, though the exact speed depends on the nature of the solvent as well as that of the ligand.[32]

The limitation of this antenna excitation is the wavelengths typically required to successfully sensitize the metal are close to UV region of the spectrum.[33, 34] This could be circumvented through the use of a two-photon absorbing ligand, which would allow excitation in the red to NIR region, while still resulting in the characteristic emission from the lanthanide.[35, 36]

Herein is detailed the characterization of a novel fluorenyl-based two-photon absorbing ligand and a series of lanthanide complexes. Molecules bearing a fluorene moiety have been shown to have respectable two-photon absorbing properties, especially when combined as part of a donor-π-acceptor chromophore.[37, 38]

Experimental

Linear Photophysical Measurements

Steady-state absorption spectra were recorded on an Agilent 8453 UV-vis spectrophotometer in 10 mm path length quartz cuvettes with concentrations ~10^{-6} M in spectroscopic grade cyclohexane (CHX) and tetrahydrofuran (THF). Steady state fluorescence emission and excitation anisotropy spectra were measured with a PTI QuantaMaster spectrofluorimeter in 10 mm spectrofluorometric quartz cuvettes with concentrations ~10^{-6} M. Fluorescence emission spectra were corrected for the spectral responsivity of the PTI detection system and solvent background. Excitation anisotropy measurements were performed in an "L-format" configuration in the viscous solvent poly(tetrahydrofuran) (pTHF).[9] The PTI QuantaMaster spectrofluorimeter was fitted with a red-sensitive photomultiplier (PMT) tube to record emission below 800 nm, and an InGaAs near-infrared detector for 800-1600 nm luminescence detection. Emission spectra for the ligand and europium, samarium, terbium, dysprosium, and gadolinium complexes were recorded using the red PMT. The emission spectra of the neodymium, ytterbium, and erbium complexes were

recorded using a combination of the two detectors, for the residual ligand emission and the lanthanide emission, respectively. The values of fluorescence and luminescence quantum yields were obtained by a relative method using 9, 10-diphenylanthracene (DPA) in cyclohexane as the standard.[9]

Fluorescence lifetime measurements of the ligand was performed on a PicoHarp 300 system using a Coherent Mira 900 Ti:sapphire laser tuned to 800 nm and passed through a second harmonic generator to give 400 nm as the excitation source, and an avalanche photodiode, fitted with a suitable filter to block any scattered light, as the detector.

Time gated/phosphorescence and lifetime measurements of the lanthanide complexes were performed on a FluoroMax-P spectrofluorometer. Low-temperature measurements were achieved with a homemade optical fiber bundle probe coupled to the spectrofluorometer.[39] The distal end of the bundle was immersed in a 400 μL sample (10^{-4} M in cyclohexane) contained in a 12 x 32 mm glass vial. The probe with attached sample vial was immersed in liquid nitrogen and allowed to freeze at least 90 seconds before measurements were taken. The lifetimes of the NIR emissions of the ytterbium, neodymium, and erbium complexes were performed on an Edinburgh Instruments FLS 980

spectrofluorimeter fitted with a liquid-nitrogen-cooled Hamamatsu R5509-73 NIR PMT.

The quantum yields of the photochemical decomposition, Φ_{Ph}, of **1** and **2-Eu** were determined via one-photon excitation using a LOCTITE 97034 UV-lamp (λ_{ex} = 400 nm; $I_0(\lambda) \approx 48$ mW cm^{-2} and at λ_{ex} = 435 nm; $I_0(\lambda) \approx 27$ mW cm^{-2}). Photodecomposition quantum yields, $\boldsymbol{\Phi}_{Ph}$, were calculated using Equation 3.[15]

Nonlinear Optical Measurements

Two-photon absorption spectra of the ligand and europium complex were measured over a broad spectral region by an open aperture z-scan method using a femtosecond laser system (Coherent Inc, Figure 9).[14] Concentrations of the investigated samples were in the range 10^{-2} to 10^{-3} M. The 800 nm output of a Mira 900-F Ti:sapphire laser, with a repetition rate, f = 76 MHz and average power ≈ 1.1 W and pulse duration, $\tau_P \approx 200$ fs), pumped by the second harmonic of CW Nd^{3+}:YAG laser (Verdi-10), was regeneratively amplified with a 1 kHz repetition rate (Legend Elite USP) providing ≈ 100 fs pulses (FWHM) with energy ≈ 3.6 mJ pulse^{-1}. This output at 800 nm was split into two separate beams with average power ≈ 1.8 W each and pumped two ultrafast optical parametric

amplifiers (OPerA Solo (OPA), Coherent Inc.) with a tuning range 0.24–20 μm, τ_P ≈ 100 fs (FWHM), and pulse energies, E_P, up to ≈ 100 mJ. A single laser beam from the first OPA was used for direct 2PA cross-section measurements by the open-aperture z-scan method.[40]

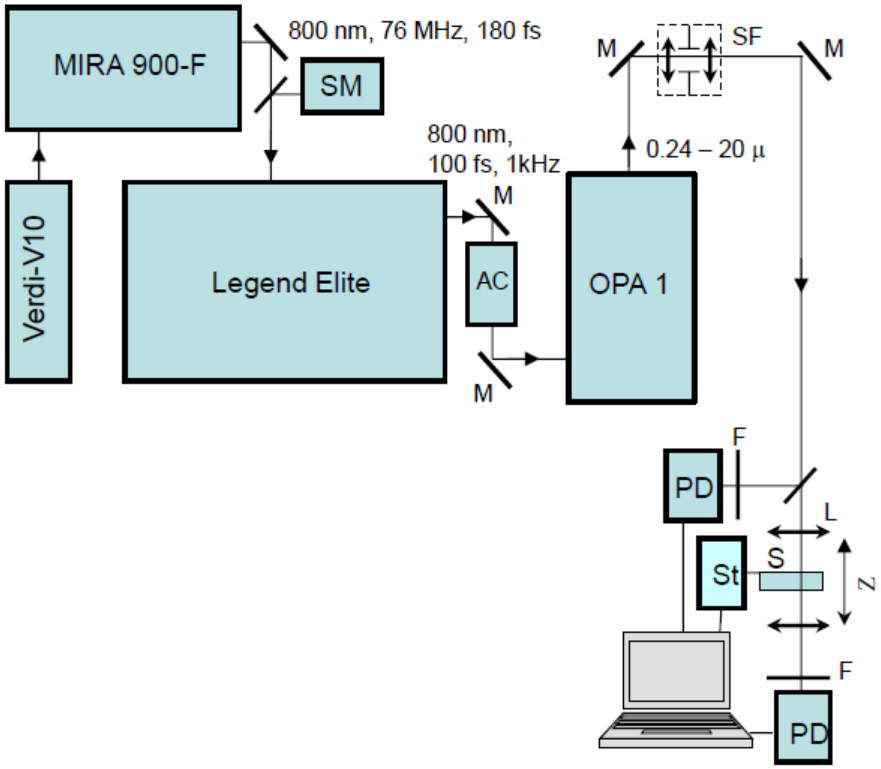

Figure 9: Experimental set up used for nonlinear absorption measurements. [Reproduced with permission from reference [41], copyright 2013 American Chemical Society.]

Two-photon upconverted fluorescence measurements were performed using the previously detailed PTI QuantaMaster spectrofluorimeter, drawing the

excitation light from a Coherent Mira 900 laser system mode-locked to 800 nm. The pulse width of the laser was 200 fs with a repetition rate of 76 MHz and 700 mW average output power. Fluorescence measurements were performed in 10 mm quartz cuvettes with dye concentrations 10^{-4} M.[42] To avoid the possibility of reabsorption, laser intensity was less than 100 mW, and was focused on the edge of cuvette closest to the detector.

Results and discussion

Synthesis

Scheme 1 shows the synthetic procedure that was used to generate the ligand and then complex it to the various metal centers (Ln= Eu, Sm, Dy, Tb, Nd, Yb, Er, Gd). Compound A was reached as previously reported.[37, 43, 44] Both ligand and complexes were characterized using elemental analysis and high-resolution mass spectrometry, with ^{1}H and ^{13}C NMR spectroscopy also applied to the ligand and europium and samarium complexes; the other metallic centers exhibit paramagnetism that distorted the spectra beyond comprehensibility.

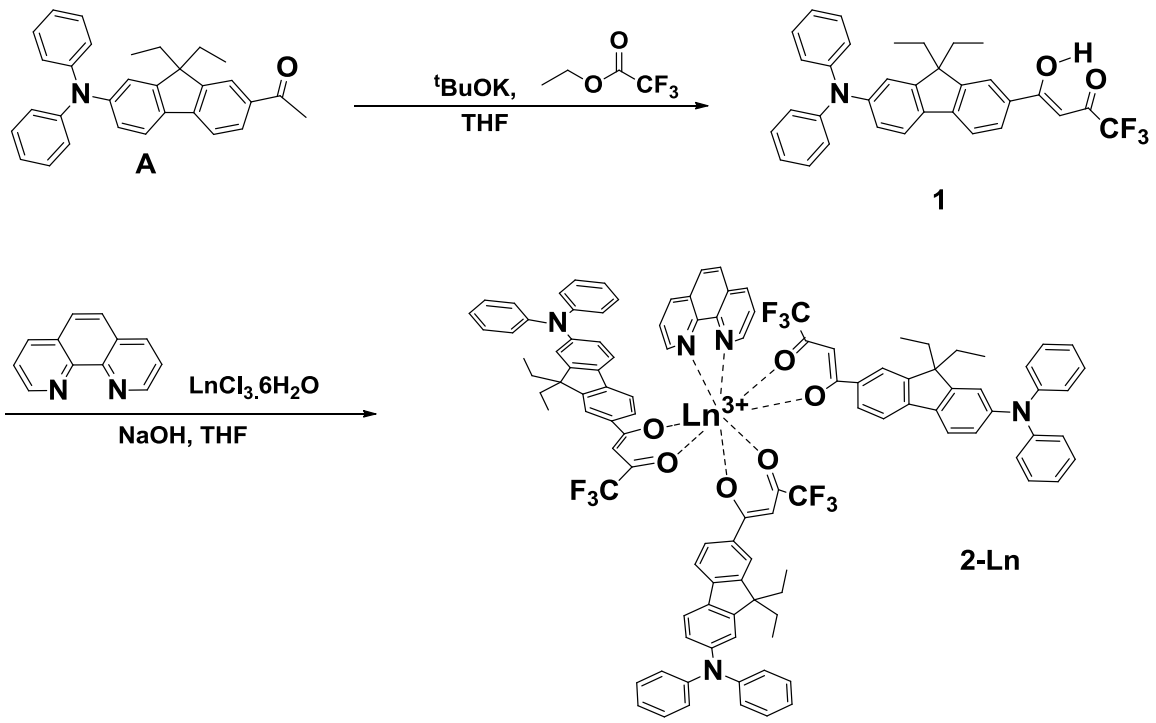

Scheme 1: Synthesis pathway for ligand **1** and lanthanide complexes **2-Ln**.

Linear Photophysical Characterization

The primary photophysical parameters for **1** in organic solvents of different polarities at room temperature are presented in Table 1. In contrast to weak solvent-dependence of the absorption spectra, the ligand shows notable solvatochromic emission behavior. Upon increasing the solvent polarity, the absorption and the fluorescence maximal wavelengths shows a systematic increase in bathochromic and Stokes shift. As shown in Figure 10, fluorescence

spectra in the polar solvent THF displayed a broad structureless emission band centered at 618 nm with large Stokes shift while those in non-polar cyclohexane exhibited a vibrational structure.[45, 46] This indicates that the nature of the excited electronic state in polar solvents is different. Increased polarity is also accompanied by significant decrease in the fluorescence quantum yield, behavior consistent with the intramolecular charge transfer (CT) character of the S_1 state.[47]

Table 1: Photophysical properties of **1** in cyclohexane and THF, with a polarity factor $\boldsymbol{P(\epsilon)}$

	$\boldsymbol{P(\epsilon)}$*	$\boldsymbol{\lambda_{max}^{abs}}$ [a] /nm	$\boldsymbol{\lambda_{max}^{em}}$ [a] /nm	$\boldsymbol{\Delta\lambda}$ [b] /nm	$\boldsymbol{\varepsilon}$ [c] /10^3 M^{-1} cm^{-1}	$\boldsymbol{\Phi_f}$ [d]	$\boldsymbol{\tau_f}$ [e] /ns	$\boldsymbol{\Phi_{Ph}}$ /10^{-6}
CHX	0.254	434	478	44	36.1	1.0	2.28	2.7
THF	0.688	439	618	179	28.0	0.64	3.24	23

[a] Absorption and emission maxima ±1 nm; [b] Stokes shift ±2 nm; [c] extinction coefficients ±5%; [d] fluorescence quantum yields ±10%; [e] fluorescence lifetimes ±10%; [f] not determined.

*Polarity factor calculated using Equation 9, where ϵ is the dielectric constant.[36]

$$\boldsymbol{P(\epsilon) = \frac{\epsilon - 1}{\epsilon + 2}} \qquad \textbf{(9)}$$

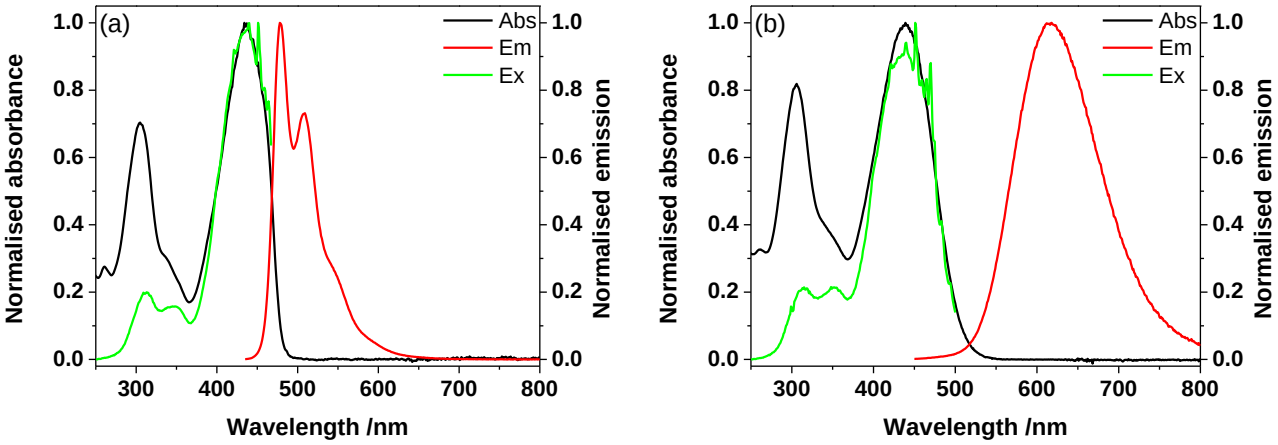

Figure 10: Absorption (black), excitation (green), and emission (red) spectra of **1** in cyclohexane (a) and THF (b) at room temperature (λ_{ex} = 440 nm, λ_{em} = 478 nm (cyclohexane); 618 nm (THF)).

The fluorescence excitation spectra of **1** in cyclohexane and THF are identical to their linear absorption counterpart (Figure 10). The absorption band centered at 434 nm in cyclohexane is similar to the absorption band centered at 439 nm in THF, a result of the absorptive transition from the ground state $S_0 \rightarrow S_1$ state, which undergoes efficient vibrational relaxation upon one-photon excitation. It is also apparent that the $S_0 \rightarrow S_2$ excitation is a less efficient process, given the difference between the excitation peak maxima at ca. 440 nm ($S_0 \rightarrow S_1$) relative to those of the absorptive transition at ca. 305 nm ($S_0 \rightarrow S_2$) in cyclohexane and THF.

Time-resolved fluorescence decays were measured in the same solvents to probe the excited state dynamics of ligand **1**. Excitation in the charge transfer

band at ca. 435 nm resulted in the fluorescence decay profiles that were monitored at the emission maximum. The fluorescence decays of ligand **1** were mono-exponential (Figure 11), indicating that the emission occurs from a single species. The fluorescence lifetime in cyclohexane was determined to be 2.28 ns, which is shorter than that observed in the more polar THF (3.24 ns). The red-shifted emission band in the fluorescence spectra of **1** in polar solvents, coupled with the increased excited state lifetimes, supports the presence of charge transfer states in **1**.

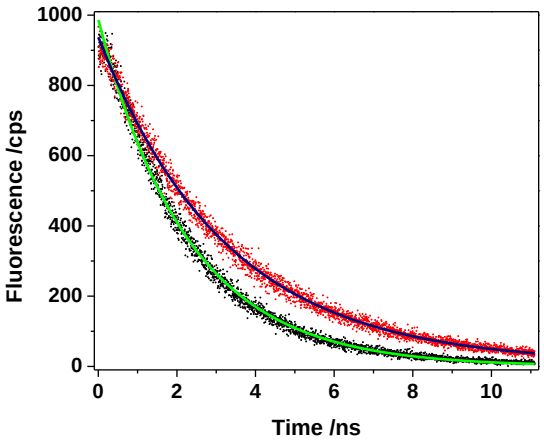

Figure 11: Fluorescence decay curves for ligand **1** in cyclohexane (black points) and THF (red points), and their fitted exponential functions (green line, and navy line, respectively).

The absorption spectra of the **2-Ln** complexes are depicted in Figure 12 along with that of **1**. The absorption spectra of the complexes in both cyclohexane and THF were similar to that of the ligand in the corresponding solvents, indicating that the singlet excited states of the ligand is not significantly affected by complexation to the Ln^{3+} ions.[48, 49] In addition, it can be noted that, once complexed, the character of the metal has limited bearing on the electronic properties of the complex as the absorption spectra for the eight metals overlay with one another.[50]

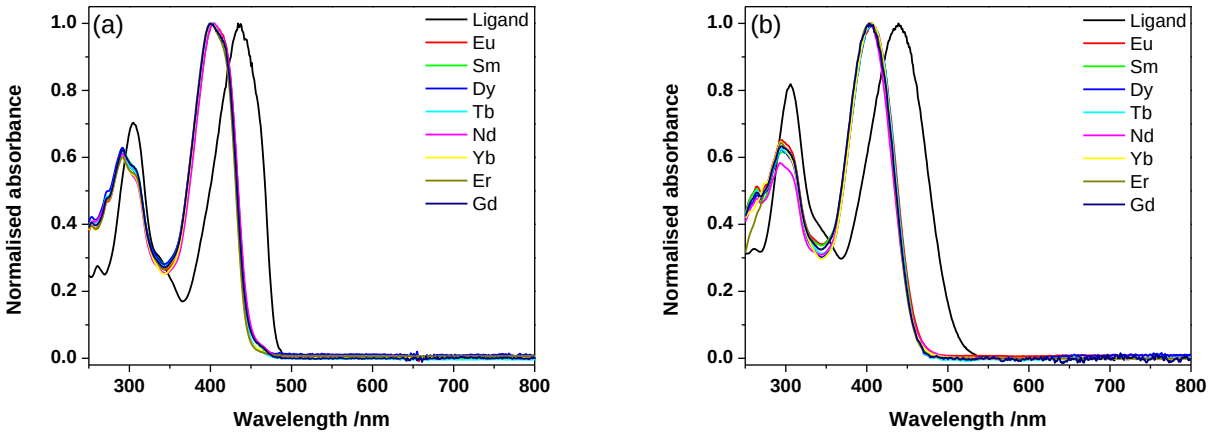

Figure 12: Normalized absorption spectra for **1** and the eight lanthanide complexes (**2-Ln**) in cyclohexane (a) and THF (b).

The main absorption band of the ligand, on complexation to the lanthanides, underwent a hypsochromic shift of ~35-40 nm in both cyclohexane and THF

(Figure 12, Table 2), while the short wavelength band (ca. 300 nm) remains unaffected. This suggests that the strength of the acceptor moiety (diketonate-CF_3) of the ligand has been decreased by the imposed negative charge of deprotonation and presence of the Lewis acidic metal center, while the donor (diphenylamino) retains the same strength. Complexation also realized an approximate three-fold increase in the extinction coefficients (~105 x 10^3 dm^3 mol^{-1} cm^{-1}), indicative of an assembly of three ligands in one complex unit. These values are within experimental error.

Table 2: Photophysical properties of the series of lanthanide complexes **2-Ln**.

2-Ln	λ_{max}^{abs} **/nm**		ε **/10^3 M^{-1} cm^{-1}**		λ_{max}^{em} **/nm**		Φ_l	
	CHX	THF	CHX	THF	CHX	THF	CHX	THF
2-Eu	405	406	109	102	478	500	0.17	0.10
2-Sm	404	405	107	93	477	500	0.15	0.13
2-Dy	403	405	115	100	476	501	0.09	0.07
2-Tb	402	408	104	102	477	504	0.15	0.07
2-Nd	405	403	111	100	477	498	0.35	0.09
2-Yb	403	405	114	106	478	502	0.29	0.05
2-Er	400	404	127	91	478	498	0.09	0.11
2-Gd	399	405	113	95	477	498	0.17	0.11

Overall luminescent quantum yields (Φ_l, incorporating lanthanide emission that emits in the visible) ranging from 0.05-0.35 were observed for the complexes on excitation into the ligand CT band at 405 nm (Table 2). Figure 13 shows the

emission spectra of **2- Eu** in cyclohexane and THF. The luminescence spectra of the complex in cyclohexane showed higher sensitization as evidenced by the strong metal-centered luminescence, accompanied by increased quenching of the ligand-centered fluorescence band, more dramatic than that observed in the more polar THF. This suggests that the energy transfer in these complexes is influenced by the solvent polarity, possibly due to a change in the conformation of the ligand. Given the similarity of the electronic structure of the synthesized lanthanide complexes, **2-Eu** was selected for additional characterization as it is possible to determine the sensitization of the metal through established methods (Table 3).

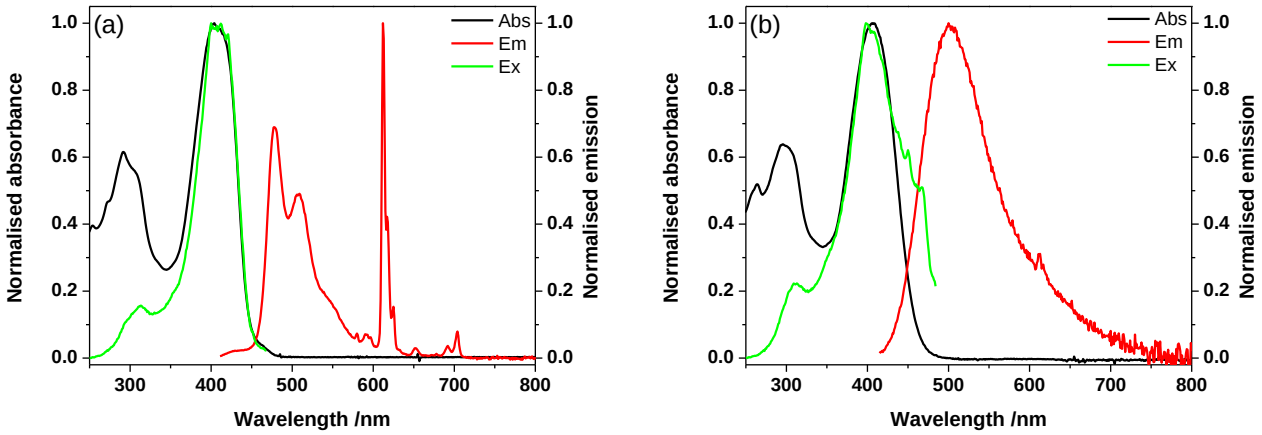

Figure 13: Absorption (black), excitation (green), and emission (red) spectra of 2-Eu in cyclohexane (a) and THF (b) at room temperature. (λ_{ex} = 405 nm, λ_{em} = 611 nm.)

Table 3: Photophysical properties of **2-Eu** in cyclohexane and THF, with a polarity factor $\boldsymbol{P(\epsilon)}$.

	$\boldsymbol{P(\epsilon)}$*	$\boldsymbol{\lambda_{max}^{abs}}$ [a] /nm	$\boldsymbol{\lambda_{max}^{em}}$ [a] /nm	$\boldsymbol{\Delta\lambda}$[b] /nm	$\boldsymbol{\varepsilon}$ [c] /10^3 M^{-1} cm^{-1}	$\boldsymbol{\Phi_l}$ [d]	$\boldsymbol{\tau_l}$ [e] /μs	$\boldsymbol{\Phi_{Ph}}$ /10^{-6}
CHX	0.254	405	478	73	109	0.17	85	26
THF	0.688	406	500	94	102	0.10	48	14

[a] Absorption and emission maxima ±1 nm; [b] Stokes shift ±2 nm; [c] extinction coefficients ±5%; [d] luminescence quantum yields ±10%; [e] luminescence lifetimes ±10%; [f] not determined.

The excitation spectrum of **2-Eu** monitored at 611 nm (corresponding to $^5D_0$ - $^7F_2$ transition of Eu^{3+}), closely resembled the corresponding absorption spectra (Figure 13). The emission spectrum obtained in cyclohexane exhibited the five bands expected for the $^5D_0 \rightarrow {}^7F_J$ (J = 0-4) transitions (Figure 13a), with a very intense $^5D_0 \rightarrow {}^7F_2$ transition, and the excitation spectrum registered at each of the emission bands exhibited a good match to the absorption spectrum (Figure 14). The highlight of the emission was focused on this hypersensitive ΔJ = 2 band, the emitted red light within this narrow wavelength region was intense. Energy transfer from the ligand to the metal in this complex is likely to be facilitated by a favorable overlap integral between the ligand donor states and the acceptor states on the europium (III) ion that are $^5D_2$ (21300 cm^{-1}), $^5D_1$ (19000 cm^{-1}) and emissive $^5D_0$ (17400 cm^{-1}) states.

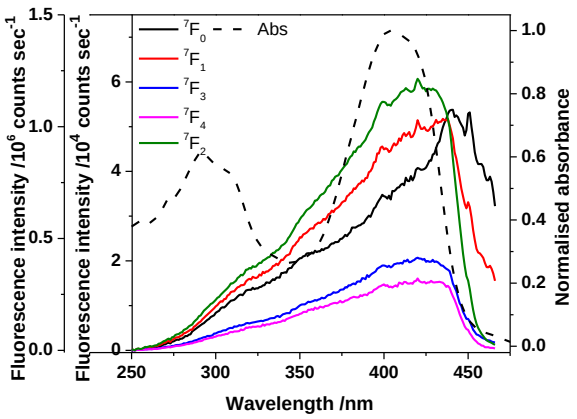

Figure 14: Fluorescence excitation spectra for **2-Eu**, monitoring the emission of each of the transitions visible in the Eu^{3+} emission ($^7F_2$ is plotted on the outer left axis for scaling purposes) in comparison to the absorption spectrum for the complex (black dashed line).

It is generally acknowledged that sensitization of lanthanide luminescence usually proceeds via the triplet state of the chromophore, although direct sensitization from the singlet state has also been observed.[33, 51] To probe the position of this triplet, **2-Gd** was synthesized and compared with the europium complex in cyclohexane at 77 K. Gd^{3+} cannot receive energy from most organic ligands because the energy level of its lowest excited state is too high (about 32000 cm^{-1}).[52, 53] Consequently a Gd^{3+} complex can be used as a model to study the ligand luminescence in the presence of heavy atom but in the absence of energy transfer. In the emission spectrum of **2-Gd**, a moderately strong emission band

emerged at 580 nm (Figure 15). Time-resolved analysis proved it to be a phosphorescent band (lifetime 1.02 ms). From this band, determination of the triplet energy of ligand **1** was determined to be 17240 cm^{-1}. The difference between this value and the energy of the $^5D_0$ emissive state of Eu^{3+} can be seen to be within experimental error.

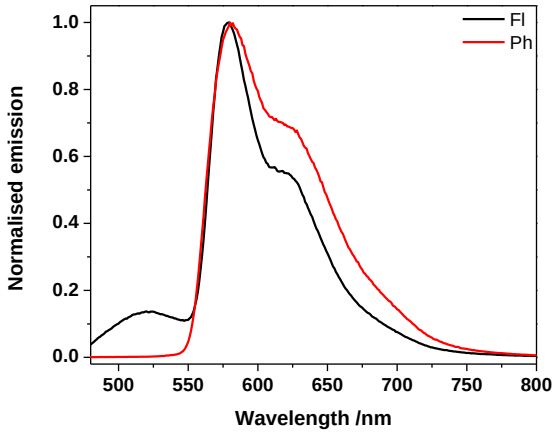

Figure 15: Fluorescence spectrum (λ_{ex} = 449 nm, black line), and phosphorescence spectrum collected after a 50 μs delay (λ_{ex} = 419 nm, red line) of **2-Gd** in CHX at 77 K.

The emission of Eu^{3+} consists of a combination of magnetic and electronic dipole transitions, and since the only detectable magnetic dipole transition ($^5D_0$ → $^7F_1$) is unaffected by its environment, it can be utilized as an internal standard in evaluating the efficiency of sensitization.[54] This is examined through Equation

10, where Φ_L^{Eu} and Φ_{Eu}^{Eu} are the ligand sensitized and intrinsic luminescence quantum yields of Eu^{3+}, respectively, η_{sens} is the sensitization efficiency, and τ_{obs} and τ_{rad} are the observed and radiative lifetimes of Eu^{3+}, respectively. Given the difficulty in direct determination of the intrinsic quantum yield of the lanthanide, due to weak absorption of f-f excitation bands, the radiative lifetime was calculated separately.[53] This was done with Equation 11, where τ_{rad} is the probability of the spontaneous emission for the $^5D_0 \rightarrow {}^7F_1$ transition in a vacuum (14.65 s^{-1}), n is the refractive index of the medium, and I_{tot}/I_{MD} is the ratio between the total integrated area of the corrected Eu^{3+} emission and the integrated intensity of the magnetic dipole $^5D_0 \rightarrow {}^7F_1$ transition.[52]

$$\boldsymbol{\Phi_L^{Eu} = \eta_{sens} \times \Phi_{Eu}^{Eu} = \eta_{sens} \times \left(\frac{\tau_{obs}}{\tau_{rad}}\right)} \quad \textbf{(10)}$$

$$\boldsymbol{\frac{1}{\tau_{rad}} = A_{MD,0} \times n^3 \times \left(\frac{I_{tot}}{I_{MD}}\right)} \quad \textbf{(11)}$$

Excluding the residual ligand emission, which contributes to the quantum yield given in Table 3, a sensitized quantum yield of 0.046 was determined, and from here the efficiency of Eu^{3+} sensitization was found to be 99%.

Nonlinear Photophysical Characterization

The two-photon absorption spectrum for **1** was acquired using the open aperture z-scan method (Figure 16) over a broad spectral region 600-1000 nm. The results revealed 2PA maximum (δ_{2PA}) ≈165 GM at λ_{ex} 860 nm, significantly higher than that of commercial fluorescein (δ_{2PA} = 47 GM at 790 nm).[55] This peak overlays well with the main linear absorption band, meaning that the two-photon transitions are not strictly forbidden by selection rules in the primary one-photon allowed absorption band, on account of **1** being an asymmetrical chromophore.[56] Measuring the two-photon absorption in cyclohexane and THF reveals a polarity effect on the 2PA cross section values of **1**; the optical nonlinearity increased modestly in magnitude from 125 GM to over 175 GM. This indicates that dipolar fluorenyl systems, such as **1**, benefits somewhat from a more polar environment.

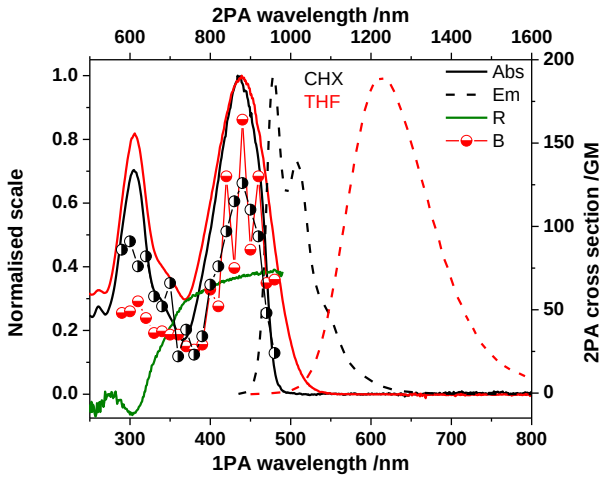

Figure 16: One and two-photon absorption (solid), emission (dash), and excitation anisotropy (dark green, in pTHF) spectra of **1** in CHX (black) and THF (red).

The two-photon absorption cross section of 340 GM at 760 nm for **2-Eu** (Figure 17) shows an approximate two-fold enhancement in the δ_{2PA} relative to 150 GM at 880 nm for ligand **1**, corresponding to the increased number of chromophores in the complex. The 2PA spectrum for **2-Eu** was only obtained in THF, as it was not possible to solubilize a sufficiently high concentration of the complex in cyclohexane.

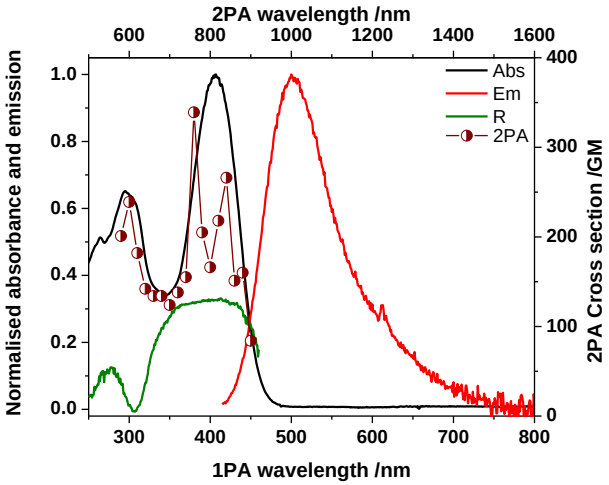

Figure 17: One (black) and two-photon (dark red) absorption, emission (red), and excitation anisotropy (dark green, in pTHF) spectra of **2-Eu** in THF.

Two-photon fluorescence spectra for **2-Eu** recorded at varying excitation powers (Figure 18) clearly show the Eu^{3+} hypersensitive $^5D_0 \rightarrow {}^7F_2$ transition at 611 nm, with the less intense satellite transitions also evident. Confirmation that the observed emission was generated by nonlinear (two-photon) excitation was seen in a comparison of the excitation power with the uncorrected integrated luminescence intensity: a quadratic correlation was observed with a 1.9 slope on a log-log plot and R^2 value of 0.99 (Figure 18, inset).

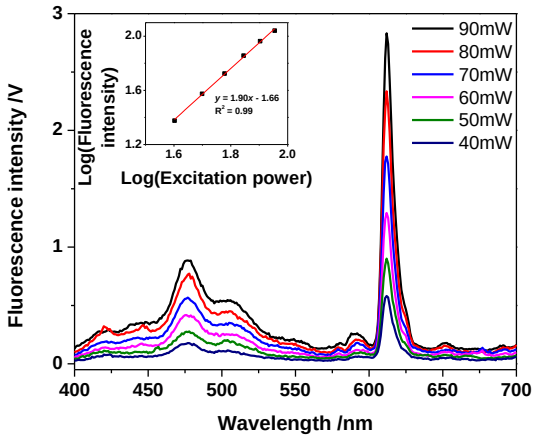

Figure 18: Two-photon upconverted fluorescence spectra of **2-Eu** in CHX excited at 800 nm recorded at incremental excitation powers; correlation of log excitation power to log integrated intensity (inset).

Conclusions

A fluorene-based donor-acceptor β-diketonate ligand was synthesized, and through characterization was found to possess charge transfer electronic states sensitive to the polarity of solvent. Using this ligand, a series of lanthanide complexes we synthesized, characterized, with **2-Eu** studied in detail. Phosphorescence studies of the ligand and **2-Gd** complex indicated that sensitization was via the triplet state. Through a combination of steady-state and time-resolved analysis of the luminescence from **2-Eu** complex, sensitization efficiency was determined to be high (99%). 2PA spectra for the ligand and

europium complex were acquired using an open aperture z-scan method, revealing satisfactory δ_{2PA} values for both **1** and **2-Eu** in THF: $\delta_{2PA} \approx 150$ GM, at λ_{ex} = 880, and $\delta_{2PA} \approx 340$ GM, at λ_{ex} = 760 nm, respectively. These values are significantly higher than that of commercial fluorescein (δ_{2PA} = 47 GM at 790 nm) and, generally, quite practical. Bathochromic luminescence was observed for the chromophore and europium complex on excitation with femtosecond lasers using 800 nm light, indicating two-photon excitation of the complex, confirmed by examining the quadratic relationship between excitation power and the luminescence spectrum of the europium complex, demonstrating efficient sensitization of the complex through two-photon excitation.

Future work

Employing two-photo excitation to access these complexes through the biological window at ~800 nm, along with the delay of these long lifetime lanthanide luminescence emissions that are present in both visible and far-IR indicate, significant potential for applications in biomedical analysis namely for imaging and sensing as luminescent probes. As such, a second generation of

ligands, along with lanthanide complexes, has been synthesized with this intent in mind.

III: BREAKING THE MIRROR PLANE – APPLYING QUANTUM CHEMICAL CALCULATIONS TO EXPLAIN PHOTOPHYSICAL PHENOMENA

Abstract

Molecular symmetry plays an important role in photophysical characterizations, as it influences the spectra obtained for a compound. However, results can sometimes be counterintuitive due to anomalous features of a molecule. In such cases, explanations cannot be inferred without additional information. In the two instances described in this chapter, the photophyscial characterization of the compounds revealed unexpected phenomena that were resolved through the use of quantum chemical calculations.

Introduction

Selection rules accompany all forms of spectroscopy, as not all molecules are capable of being detected in the same way. In the case of UV-vis absorption the two predominant rules are the conservation of spin, and the Laporte selection rule; the former requires the multiplicity of the molecule to be maintained upon

excitation, while the latter states: "The only allowed transitions are transitions that are accompanied by a change of parity."[57] This means that for a molecule that is centrosymmetric, an electronic transition can only occur between orbitals with different symmetry, i.e. gerade (g) → ungerade (u), or vice versa.[58] This is particularly prevalent in inorganic complexes, as once the *d*-orbitals split, according to the nature of ligands around the metal center, there should no longer be transitions between these orbitals. Despite these formal selection rules, transitions still manage to occur, albeit very weakly absorbing (<1000 dm^3 mol^{-1} cm^{-1}), due to the spin-orbit coupling.[59]

The influence of symmetry is important in two-photon absorption as well, however now a one-photon forbidden transition for a symmetrical molecule can be accessed through exciting by two-photons. This is because the first photon absorbed achieves a quasi-state with opposing symmetry than the ground state, and then the second photon leaves the molecule in an excited state with opposing symmetry to the quasi-state, though the same as the ground state. This results in the maximum of a two-photon spectrum appearing in a region with little absorption according to the one-photon spectrum.[60] In the case of asymmetric molecules, no such dependence exists, and one- and two-photon maxima are shown to overlap.[61]

In addition to conventional experimental techniques, quantum chemical calculations such as density functional theory, or DFT, are becoming a commonly used tool in chemistry, allowing for molecular level analysis of compounds without the need to set foot in a laboratory. The theory works through the determination of the energy of a molecule through its electron density rather than a wave function.[62]

This chapter looks at two molecules, a difluoroboron bis-β-diketonate (**3**, Figure 19) and a Janus dione derivative (**4**, Figure 19), that both present as symmetrical, though exhibit asymmetric tendencies in their two-photon absorption spectra.

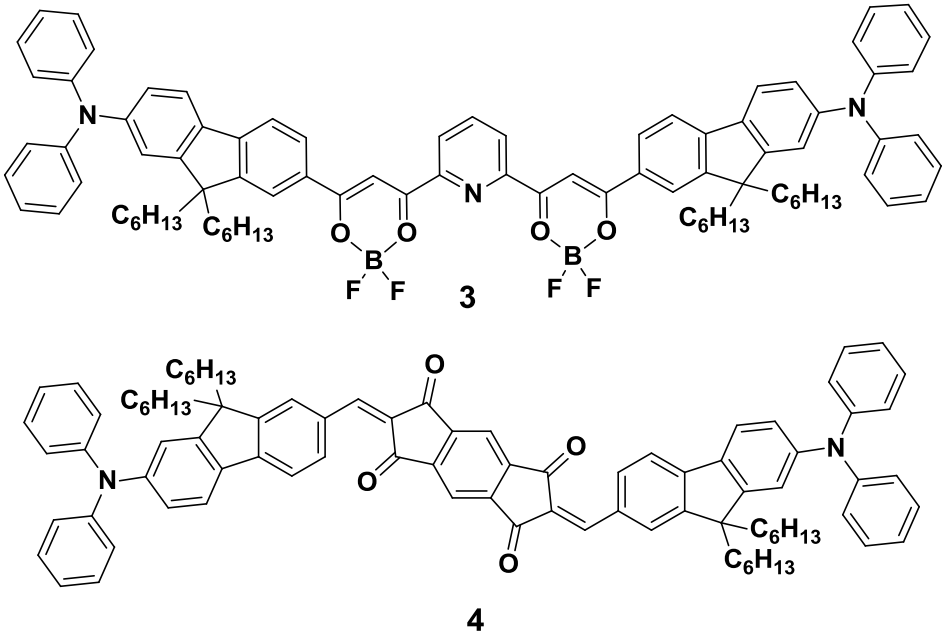

Figure 19: Structures for difluoroboron bis-β-diketonate **3** and Janus dione derivative **4**.

Organic complexes of difluoroboron have become common in the form of boron-dipyrromethene, or BODIPY, derivatives. These compounds typically show little to no solvatochromatic behavior, though their absorption spectra can be tuned through augmenting the functional groups attached to the BODIPY core.[63] β-Diketonates share many of the photophysical properties exhibited by their BODIPY cousins: high fluorescence quantum yields, and large extinction coefficients and two-photon absorption cross sections.[64]

In comparison, the indacene-1,3,5,7(2H,6H)-tetraone, or the Janus dione center of **4** has received very little attention in the literature, likely in part due to the difficulty synthesizing the moiety.[65] Despite this, results have it to be an effective component of fluorescent probes and metal sensors.[66]

Experimental

Photophysical Characterization

Absorption spectra were recorded for solutions (≈ 10^{-6} mol dm^{-3}) of the compounds in a range of solvents of differing polarity, as permitted by compound solubility, in a 1 cm quartz cuvette using an Agilent 8453

spectrophotometer. Fluorescence measurements (steady state, excitation anisotropy, and lifetime) were performed on a PTI QuantaMaster fitted with a xenon lamp and red sensitive PMT for steady state measurements, and a nitrogen-pumped dye laser and gated PMT for time-resolved measurements. Fluorescence quantum yields were measured via a relative method, using DPA as a standard. Photodecomposition quantum yields were measured via one-photon excitation using a LOCTITE 97034 UV-lamp (λ_{ex} ~ 436 nm; $I_0(\lambda)$ ≈ 56 mW cm^{-2}) for compound **3**, and a green laser diode (λ_{ex} ~ 532 nm; $I_0(\lambda)$ ≈ 90 mW cm^{-2}) for compound **4,** and calculated through Equation 3.

Degenerative two-photon absorption spectra were collected using an open aperture z-scan set-up, with a Coherent Inc. Legend amplified system seeded by a Coherent Inc. Mira Ti:sapphire laser pumping an Opera solo OPA, as previously described.[14, 61]

Quantum Chemical Calculations

Structures were prepared with the GaussView5 program, before an initial optimization of the coordinates with an AM1 calculation. This was then fully optimized using the B3LYP DFT method in the GAUSSIAN09 software package,[67]

using the D95* basis set to define the atoms. Time dependent calculations where then performed on the optimized structures with the modified M05-QX method,[68] in the case of compound **3**, and the M06 method, for compound **4**. The hexyl chains on the 9-position of the fluorene moieties were truncated to methyl groups for both molecules as they have no bearing on the photophysical properties of the chromophore, and to reduce calculation times.[69]

Results and discussion

Synthesis

Compound **3** was prepared as outlined in Scheme 2, with each intermediate structure being characterized with ^{1}H and ^{13}C NMR spectroscopy, and high resolution mass spectroscopy, with addition of elemental analysis in the case of the final product. Janus dione derivative **4** was synthesized through the route shown in Scheme 3, and each intermediary compound was confirmed in a similar manner.

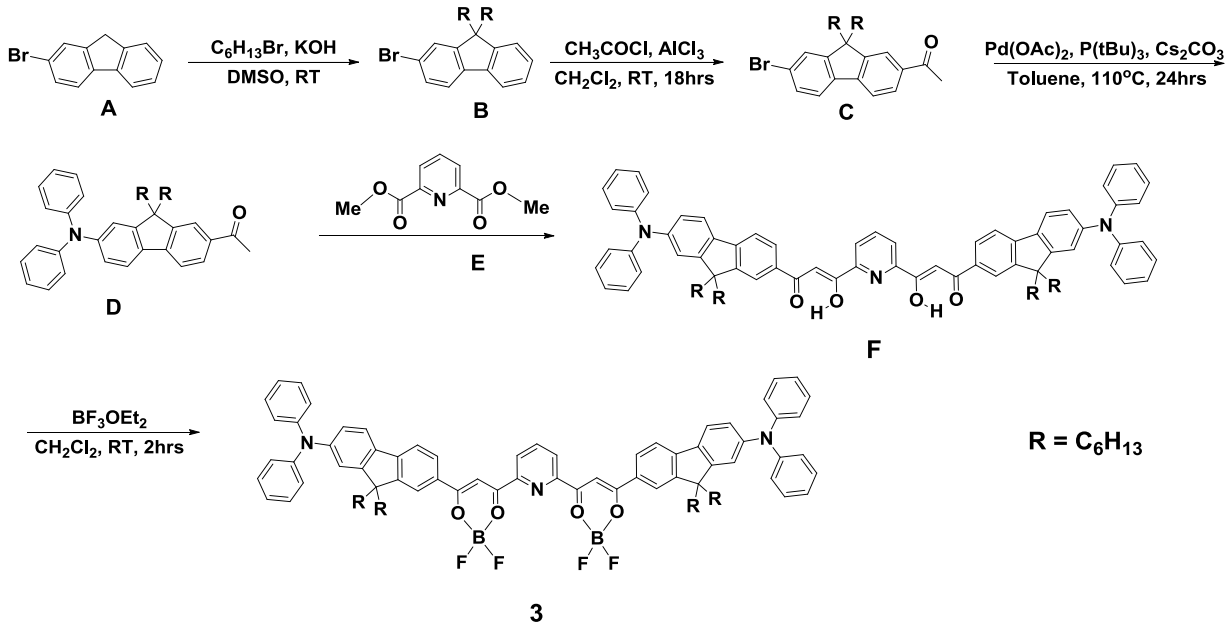

Scheme 2: Synthetic route used to obtain difluoroboron bis-β-diketonate complex **3**.

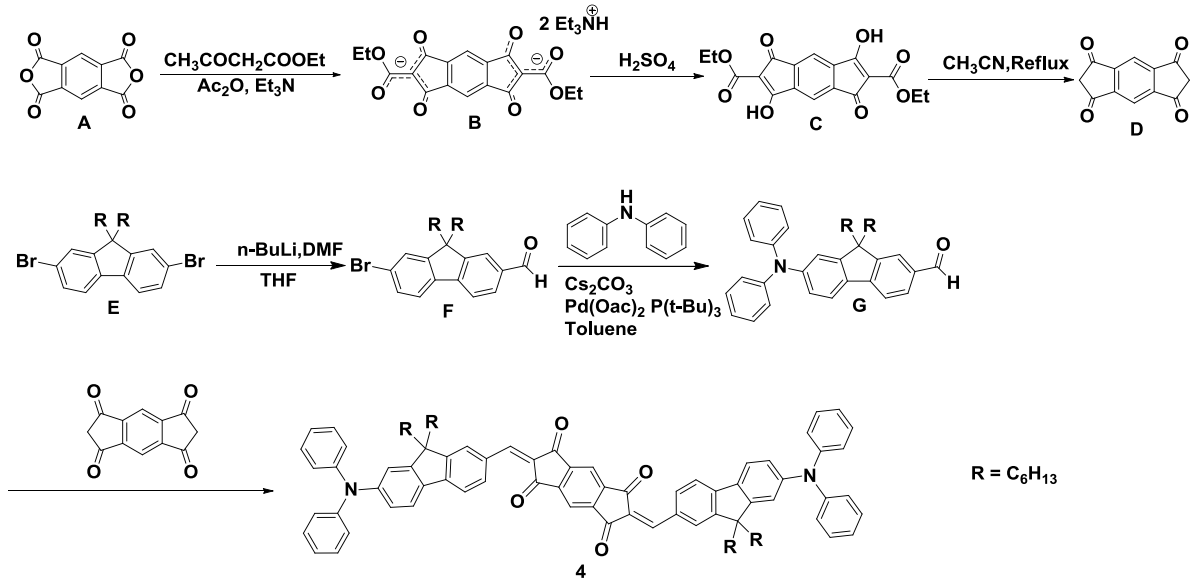

Scheme 3: Synthesis of Janus dione **4**.

Photophysical Characterization

Compound **3** exhibited two main absorption bands (Figure 20), one in the region of 500-550 nm, and one around 360-375 nm, with a near consistent ratio across solvents of increasing polarity. The emission at 550-800 nm appears to be exclusive to the non-polar solvents used (Figure 20a), while the emission between the absorbance peaks (400-500 nm) was present in all investigated solvents. Given that the excitation around 370 nm that generates this short wavelength emission also causes the longer band (albeit it at lower intensity than the long wavelength absorption gives arise to), it can be speculated that the emission arises as a result of relaxation from a higher excited state. At this state, there is relatively little energy expended in rearrangement of solvent to accommodate the dipole. However when excited in the longer wavelength band, solutions in polar solvents use more of the energy from excitation, making internal conversion to the ground state more preferable (Figure 20b).

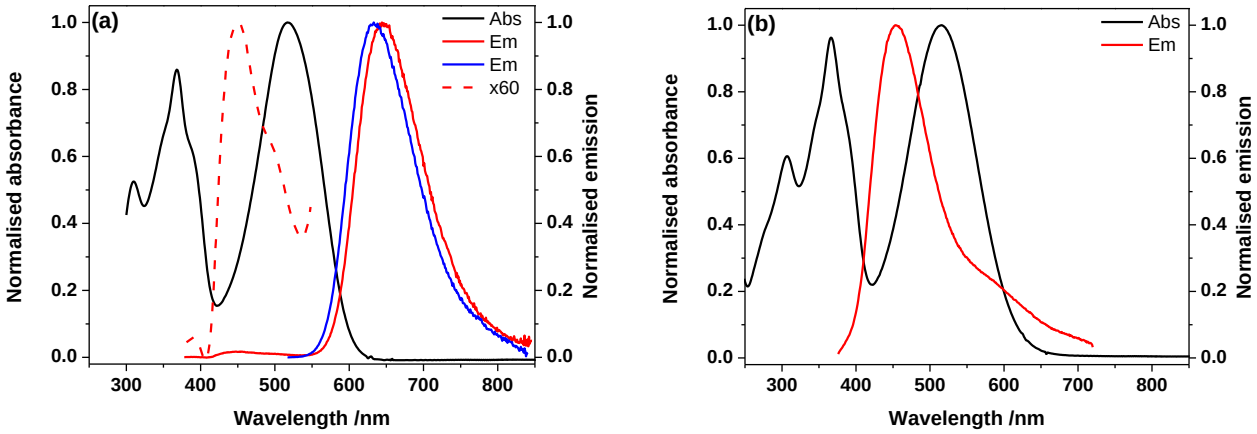

Figure 20: Absorption (black) and emission (blue and solid red) spectra for compound **3** in (a) toluene and (b) THF. The red emission is obtained through excitation at the short wavelength peak; the blue emission from the long wavelength peak. The 'x60' (dashed red) in (a) represents the enlargement of 400-550 nm region when excited at 368 nm.

Due to the overlap of the emission from the shorter wavelength peak with the absorption spectrum, the quantum yields presented in Table 4 were determined based off of the long wavelength excitation, and hence none are report for the solvents where this emission was absent. The observed decrease in quantum yield with increased polarity is consistent as the solvent is shifted from hexane, cyclohexane to toluene (Table 4). No reasoning is apparent as to why the fluorescence lifetime decreases with increased polarity, as this is counterintuitive.

Table 4: Photophysical data for difluoroboron bis-β-diketonate **3** in solvents of varying polarity.

	$\lambda_{max}^{abs\ a}$ /nm	$\lambda_{max}^{em\ a}$ /nm	$\Delta\lambda^{b}$ /nm	ε^{c} /10^3 M^{-1} cm^{-1}	$\Phi_f{}^{d}$	τ^{e} /ns	Φ_{Ph} /10^{-6}
Hex	*361*, 502	*418*, 567	*57*, 65	*55*, 50	0.91	4.3	12
CHX	*363*, 509	*425*, 573	*62*, 64	*58*, 51	0.84	4.1	2.7
Tol	*368*, 517	*450*, 644	*82*, 127	*49*, 56	0.39	2.3	0.97
DCB	*375*, 544	*484*	*109*	*54*, 47	-[f]	-[f]	0.65
DCM	*371*, 535	*482*	*111*	*41*, 36	-[f]	-[f]	1.1
THF	*366*, 516	*452*	*86*	*52*, 47	-[f]	-[f]	5.6

Italicized values relate to shorter wavelength features. [a] Absorption and emission maxima ±1 nm; [b] Stokes shift ±2 nm; [c] extinction coefficients ±5%; [d] fluorescence quantum yields ±10%; [e] fluorescence lifetimes ±10%; [f] not determined.

The absorption spectra of compound **4** in solvents of differing polarities (Figure 21) show the presence of a main absorption band centered at ~585 nm, and two smaller bands at ~400 nm and ~300 nm. Fluorescence was only observed in the toluene solution, but was intense with a quantum yield of 0.70. In the more polar solvents, the same radiationless relaxation that predominates for **3** is evident here as well (Table 5).

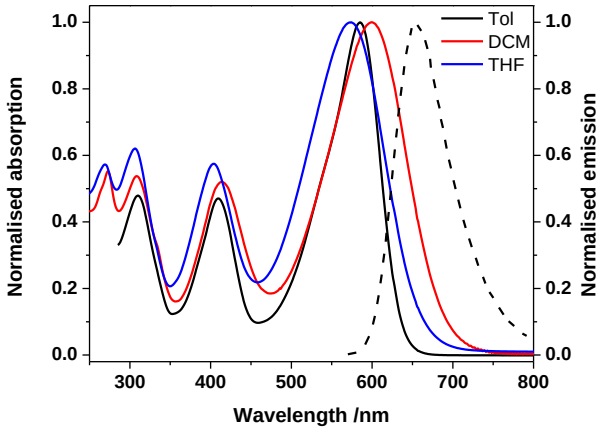

Figure 21: Absorption (solid lines) and emission spectra (dashed lines) for compound **4** in toluene, dichloromethane, and THF.

Table 5: Photophysical data for Janus dione **4** in solvents of varying polarity.

	λ_{max}^{abs} [a] /nm	λ_{max}^{em} [a] /nm	$\Delta\lambda$ [b] /nm	ε [c] /10^3 M^{-1} cm^{-1}	Φ_f [d]	τ [e] /ns	Φ_{Ph} /10^{-6}
Tol	585	655	70	83.9	0.70	2.9	0.32
DCM	591	- [f]	- [f]	72.1	- [f]	- [f]	0.99
THF	574	- [f]	- [f]	65.2	- [f]	- [f]	8.7

[a] Absorption and emission maxima ±1 nm; [b] Stokes shift ±2 nm; [c] extinction coefficients ±5%; [d] fluorescence quantum yields ±10%; [e] fluorescence lifetimes ±10%; [f] not determined.

In the case of both compound **3** and **4**, the photodecomposition quantum yields determined are consistent with those of other fluorenyl based fluorescent probes that have been investigated.[70, 71]

The excitation anisotropy trace obtained for bis-β-diketonate **3** (Figure 22a) shows a slight distortion in the plateau through the main absorption band. However this only becomes evident when the trace is expanded, and so could be an effect of noise. The anisotropy trace recorded for **4** (Figure 22b) also lacks a plateau in the main absorption band, instead displayed an increase, leading to the belief that multiple transitions are represented by the band, as well as hinting at a two-photon allowed transition.[71]

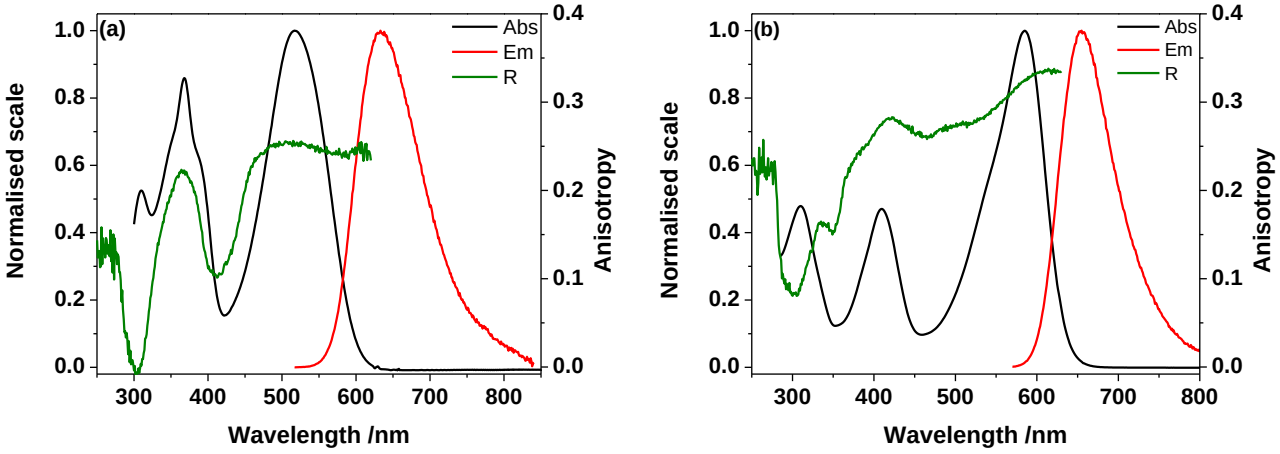

Figure 22: Absorption (black) and emission (blue) spectra in toluene, and excitation anisotropy (dark green) in silicone oil for compounds **3** (a) and **4** (b).

The two-photon absorption spectrum of **3** was recorded in toluene and THF (Figure 23). The position of the two-photon absorption maximum (λ_{max}^{2PA}) overlays with that of the one-photon spectrum, suggesting that the same excited state is

reached, regardless of the excitation mode. This result was unforeseen, as compound **3** appears to possess a plane of symmetry through its pyridine ring. Despite this, the 2PA spectrum is shown to be independent of solvent polarity, as this data shows good overlap across the two solvents.

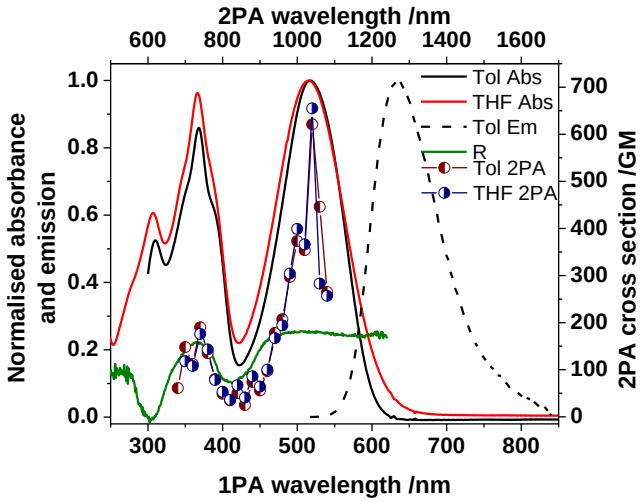

Figure 23: Absorption (toluene, solid black; THF, red), emission (toluene, dashed black), excitation anisotropy (silicone oil, dark green), and two-photon absorption (toluene, dark red points; THF, dark blue points) spectra for compound **3**.

For compound **4**, the two-photon absorption measurements were performed for a toluene solution (Figure 24). The maximum for this spectrum shows reasonable agreement with the linear absorption spectrum, albeit slightly hypsochromically shifted from it. This is similarly counterintuitive given that the structure of compound **4** appears symmetrical.

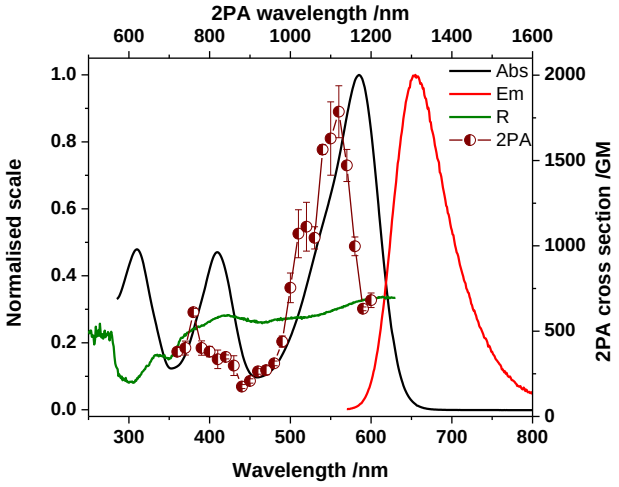

Figure 24: Absorption (black) and emission (red) spectra in toluene, excitation anisotropy in silicone oil (dark green), and two-photon absorption in toluene (dark red points) for compound **4**.

Using the data obtained from the two-photon absorption spectra, the figure of merit, F_M, can be calculated for these two compounds across the solvents used through equation 8.[25] Although the two-photon absorption spectra for **3** were recorded in toluene and THF, the maxima of the spectra were within experimental error of one another. As such the average of the maxima was used in to estimate F_M for hexane and cyclohexane (Table 6).

Table 6: Figures of merit for compounds **3** and **4**.

Compound	Solvent	F_M /10^6 GM
3	Hex	50
	CHX	200
	Tol	250
4	Tol	4200

The figures of merit for the toluene solutions show good agreement with other fluorene-based dyes that have been synthesized, which share a marked improvement over commercial dyes such as LysoTracker® Red (F_M = 0.4×10^6 GM)[24] and fluorescein (F_M = 6×10^6 GM).[25]

Quantum Chemical Calculations

Starting from the structure shown in Scheme 2, the optimized structure for compound **3** (Figure 25) shows a horseshoe-like conformation. Despite this, the structure has a high level of planarity through the main body of the chromophore (omitting the diphenylamino moieties); with a slight twist offsetting the fluorene moieties. Examination of the frontier molecular orbitals (Figure 26) reveals that the HOMO and HOMO-1 bear a striking resemblance to one another, differing only in some minor details and the diphenylamino-fluorene branch they rest upon. Similitude is also seen in the shape and the

positioning of the LUMO and LUMO+1, outside of the pyridine. The distribution of these orbitals confirms the donor-π-acceptor design of the molecular, as the electron density can be seen to shift from the diphenylamino to the 2-6-bis-β-diketonate pyridine upon excitation from HOMO to LUMO. Further analysis of the energies for these orbitals confirms their proximity (Figure 26).

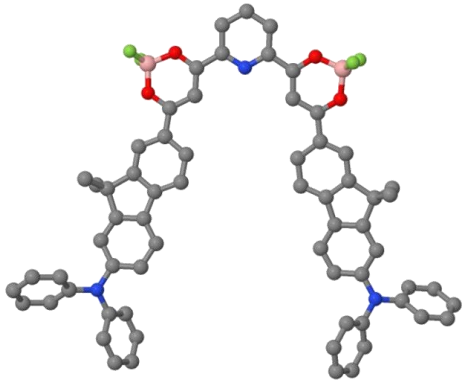

Figure 25: Optimized structure for compound **3**.

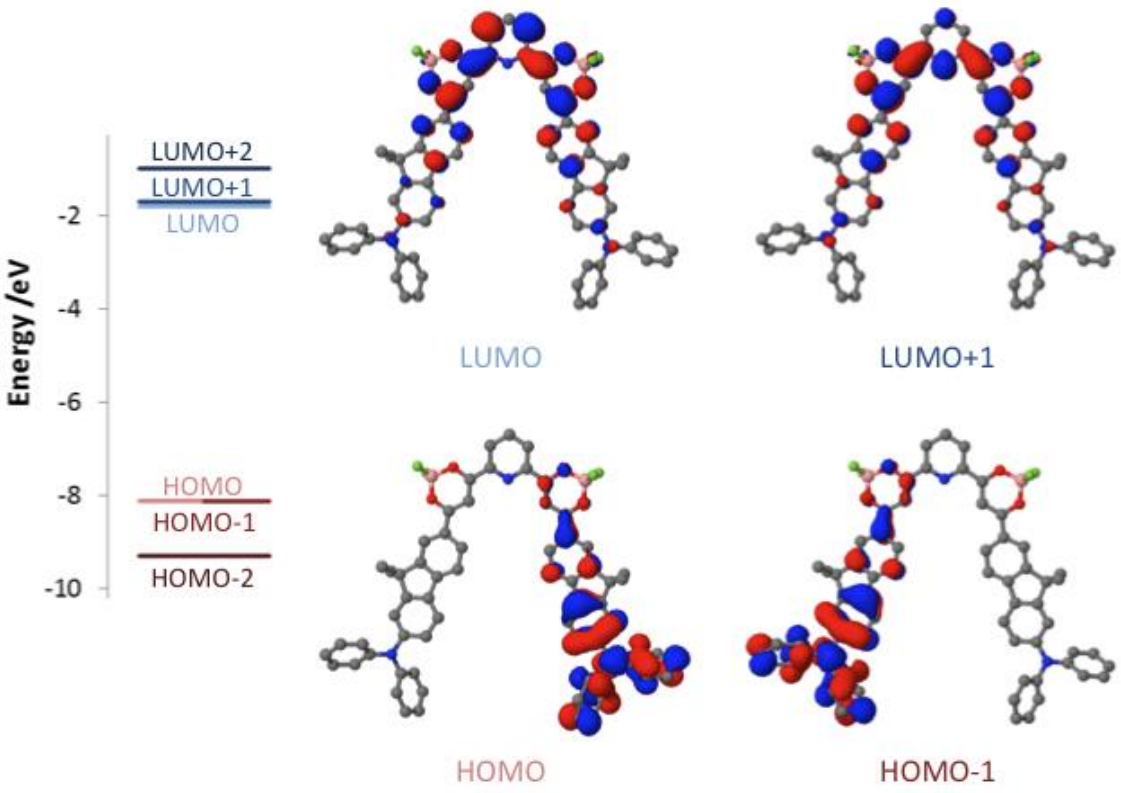

Figure 26: Frontier molecular orbitals for compound **3**, and their respective energies.

Compared to compound **3**, little change was seen in the conformation going from the initial structure to the optimized form of **4** (Figure 27, center). The central part of the molecule exhibits a very high level of planarity, with the diphenylamino moieties giving the structure most of its depth. Transitioning from the HOMO to LUMO (Figure 27), the electron density transfers away from the diphenylamino donor to Janus dione moiety in the center. The HOMO and HOMO-1 have minor differences in shape, but differ in the phase on one side of

the molecule. With this, and the appearance of the other orbitals, it is possible to label each as gerade or ungerade (Figure 27).

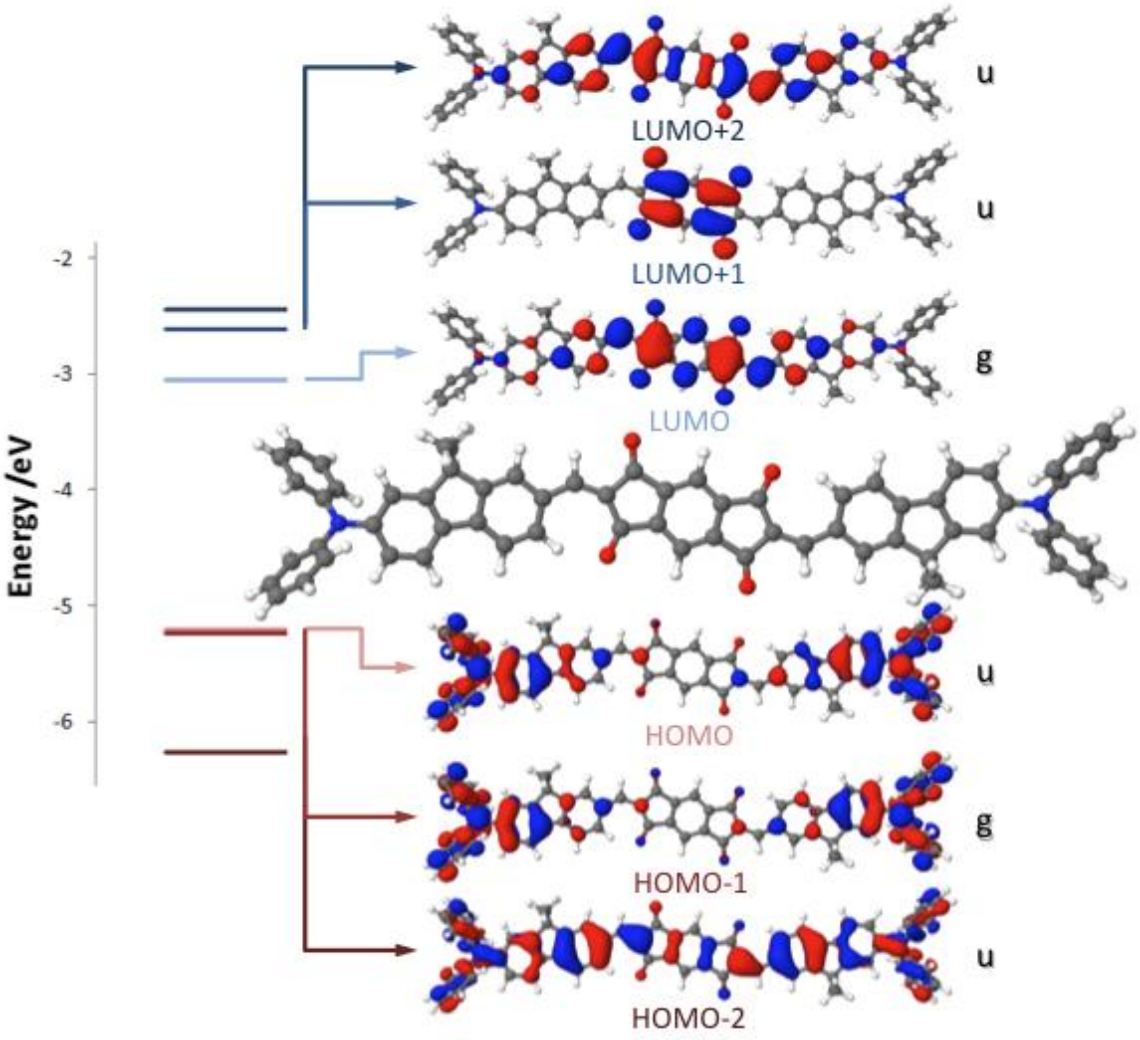

Figure 27: Optimized structure (center) and frontier molecular orbitals labeled as gerade or ungerade for compound **4**.

Analysis of the results from the TD-DFT calculation for compound **3** (Figure 28), uncovers the transitions within the main absorption band: an amalgam of excitations from HOMO and HOMO-1 to LUMO and LUMO+1, with varying degrees of prevalence (Table 7). Figure 28 also included a calculated two-photon absorption spectrum for **3**, determined through the use of the transition and stationary dipoles for the excited states of the molecule.[68]

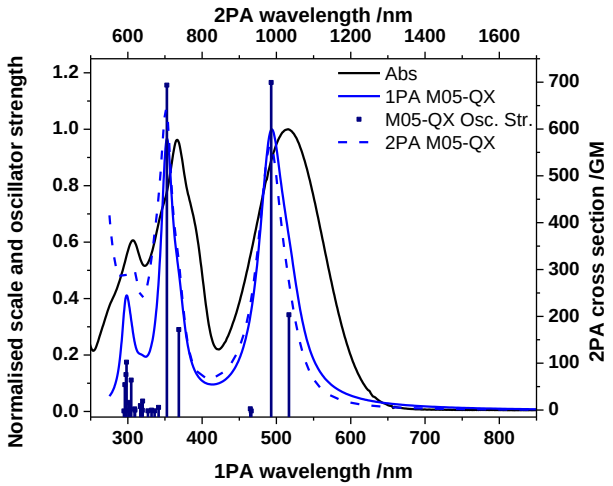

Figure 28: Calculated (solid blue) and experimental (in THF, black) linear absorption spectra, oscillator strengths (bars), and calculated two-photon absorption (dashed blue) for compound **3**.

Table 7: Molecular orbital transitions occurring within the main absorption band of compound **3**.

Wavelength /nm	Oscillator strength	Transition			Relative proportion
517	0.3425	HOMO-2	→	LUMO+1	0.02
		HOMO-1	→	LUMO	0.31
		HOMO-1	→	LUMO+1	0.14
		HOMO	→	LUMO	0.18
		HOMO	→	LUMO+1	0.29
493	1.1658	HOMO-1	→	LUMO	0.19
		HOMO-1	→	LUMO+1	0.28
		HOMO	→	LUMO	0.40
		HOMO	→	LUMO+1	0.10
466	0.0016	HOMO-1	→	LUMO	0.28
		HOMO-1	→	LUMO+1	0.09
		HOMO	→	LUMO	0.19
		HOMO	→	LUMO+1	0.43
465	0.0093	HOMO-1	→	LUMO	0.19
		HOMO-1	→	LUMO+1	0.46
		HOMO	→	LUMO	0.20
		HOMO	→	LUMO+1	0.14

In the case of **4**, the TD-DFT calculation indicates a single transition responsible for the main absorption band: HOMO → LUMO. However, at a slightly shorter wavelength, a transition is reported between HOMO-1 and LUMO, although the oscillator strength is very low (nearly 20000 times smaller), confirming that the compound is restricted by the Laporte selection rule given its symmetric nature. Transitions between HOMO-1 and LUMO+1, and HOMO and

LUMO+2 can be seen (Table 8) to be formally forbidden as well due to the symmetry of the molecule.

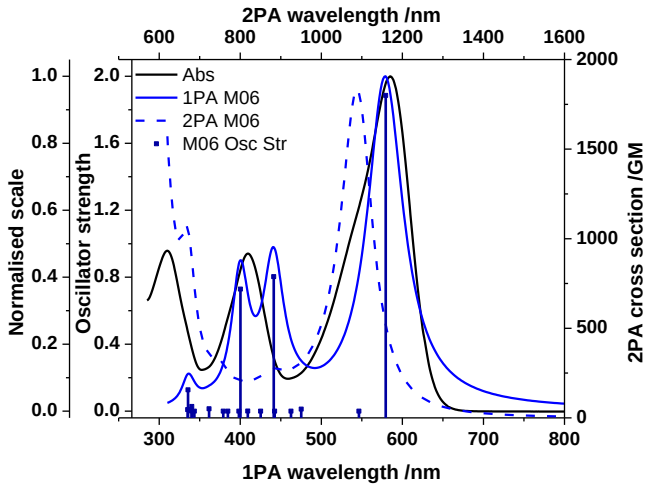

Figure 29: Calculated (blue) and experimental (in toluene, black) linear absorption spectra, oscillator strengths (bars), and calculated two-photon absorption (dashed blue) for compound **4**.

Table 8: Calculated molecular orbital transitions for compound **4**.

Wavelength /nm	Oscillator strength	Transition			Relative proportion
579	1.8856	HOMO-1	→	LUMO+2	0.04
		HOMO	→	LUMO	0.93
546	0.0001	HOMO-1	→	LUMO	0.98
475	0.0124	HOMO-2	→	LUMO+1	0.04
		HOMO	→	LUMO+1	0.95
463	0.0000	HOMO-1	→	LUMO+1	0.98
442	0.0001	HOMO	→	LUMO+2	0.96
441	0.8035	HOMO-2	→	LUMO	0.03
		HOMO-1	→	LUMO+2	0.87
		HOMO	→	LUMO	0.06

It can be noted that the calculated 2PA spectrum presented in Figure 29 displays the same hypsochromic shift from the calculated linear absorption that is seen with the experimental data (Figure 24). This δ lines ups with the one-photon forbidden transition HOMO-1 → LUMO, as predicted by the expansion of the Laporte selection rule.

Conclusions

Through the use of TD-DFT calculations, it has been possible to explain the unexpected maxima in the two-photon absorption spectra for two compounds. In the case of the difluoroboron bis-β-diketonate complex **3**, the degeneracy of the occupied molecular orbital results in an asymmetry in the ground state, allowing it be excited via two-photon into the unsymmetrical LUMO. Janus dione derivative **4** also possesses a degenerate occupied molecule orbital, however in this case it is opposite in symmetry to its highest counterpart, permitting two-photon absorption to promote an electron from this state to the equally symmetrical LUMO.

Future work

The work on difluoroboron bis-β-diketonate complex **3** has concluded with its encapsulation in micelles, a necessary step before it could be introduced into cells. Fluorescence microscopy of these cells revealed that the encapsulated dye gathered in the lysosomes of HCT-116 (human colon carcinoma) cells.

Compounds similar to the Janus dione derivative **4** have been synthesized, including variants with hydrophilic polyethyleneglycol chains in the 9-position on the fluorene moiety. At time of writing, these compounds are undergoing characterization to determine their viability for fluorescence bioimaging.

IV: COMPUTER AIDED CHEMICAL DESIGN: USING QUANTUM CHEMICAL CALCULATIONS TO PREDICT PROPERTIES FOR A SERIES OF HALOCHROMIC GUAIAZULENE DERIVATIVES

Abstract

With the scientific community becoming increasingly aware of the need for greener products and methodologies, the optimization of synthetic design is of greater importance. Starting from an already synthesized guaiazulene derivative, a series of similar structures were investigated with TD-DFT methods in an effort to select a compound with appreciable properties. Such a route eliminates the possibility of unknowingly synthesizing materials that exhibit no viable applications. Synthesis of the largest structure studied *in silico* revealed discrepancies in the calculation results. Further computational study of the molecule yielded results closer to those seen experimentally.

Introduction

The drive towards greener chemical practices has been a goal of increasing importance of the past decade. In his 1998 book, Paul Anastas features 12

principles for green chemistry, the first of which states: "It is better to prevent waste than to treat or clean waste after it is formed."[72] To this end, the use of quantum chemical calculations to provide a prediction of a compound's properties prior to generating it in the lab could help to minimize such waste caused through synthesizing impractical derivatives. The use of *in silico* techniques is commonly used to aid in the explanation of experimental results,[41, 73] though more recently studies have been directed towards identifying sustainable solvents,[74] designing solar cell components[75] and complex metal oxides.[76]

Another of Anastas's principles is for the use of chemicals with renewal sources, or otherwise coming from nature.[72] Extractable from fungi[77] and coral,[78] 1,4-dimethyl-7-isopropylazulene, or guaiazulene, is a natural derivative of azulene. Although this is an isomer of the colorless naphthalene, azulene exhibits a blue color that has enchanted man since the late medieval period.[79] It is a famed photophysical curiosity, due to it being an exception to Kasha's rule, in that its fluorescence is generated by the relaxation of $S_2 \rightarrow S_0$, due to the asymmetry of the electrons across the rings inducing a dipole of 1.08 D.[79, 80] When exposed to acidic conditions, e.g. trifluoroacetic acid (TFA), azulene derivatives show halochromic behavior; the 3-position is protonated, on the cyclopentane ring,

though the charge is delocalized to the 7-membered ring creating a tropylium ion.[81] This results in a bathochromic shift in the $S_0 \rightarrow S_1$ band of the absorption, as well as the appearance of fluorescence from the S_1 excited state.[82] When the compound is substituted through the 7-membered ring, this protonation can be reversed with the addition of triethylamine (TEA);[79] substitution of just the 5-memebered ring can result in irreversible protonation.[82, 83]

The development of long wavelength absorbing materials for use in optoelectronics[84] and solar cells[85] has become an increasing contemporary area of research. The protonated forms of azulene derivatives have shown to be potentially viable candidates for such applications, with linear absorption spectra extending into the NIR.[80]

In an effort to reach a desirable derivative without going through undesirable products, a series of molecules similar to the initially synthesized and characterized guaiazulene derivative **5** (Figure 30), and its conjugate acid **5H**, were designed and spectral properties were predicted through TD-DFT methods. Characterization of the culmination of these calculations, **6** and **6H** was then performed to verify the predictions.

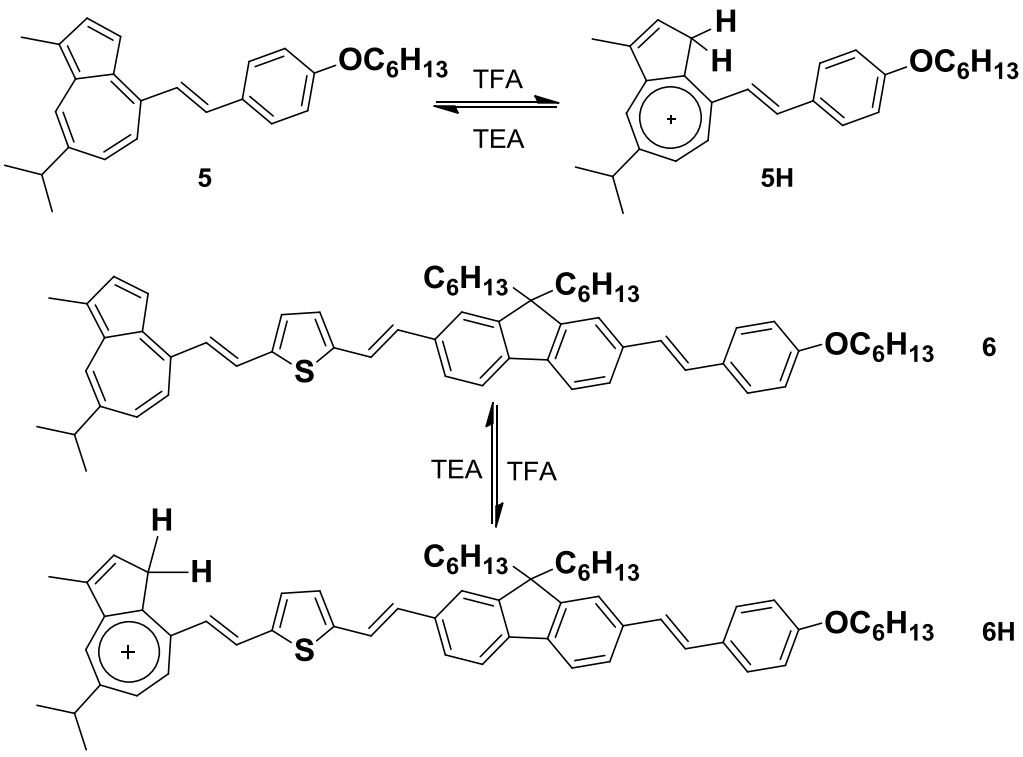

Figure 30: Structures for guaiazulene derivatives **5** and **6**, and their conjugate acids formed upon exposure to TFA, **5H** and **6H**.

Experimental

Photophysical Characterization

Linear photophysical properties were measured using prepared solutions (~ 10^{-6} M) in 10 mm quartz cuvettes using spectroscopic grade solvent. An Agilent 8453 was used to collect absorption spectra, while an Edinburgh Instruments FLS 980 for steady-state luminescence emission, excitation anisotropy, and

fluorescence lifetimes. These measurements utilized a red-sensitive PMT, and a liquid-nitrogen-cooled Hamamatsu R5509-72; all measurements were corrected for detector response.

Fluorescence quantum yields were calculated using a relative method, with DPA (Φ_f = 0.95) as a reference.[9] Anisotropy measurements were performed in a viscous solvent, namely silicone oil, to hamper the rotational relaxation of the molecules. Fluorescence lifetimes were measured using a 470 nm EPL laser for **5H** and a 670 nm EPL laser for **6H**.

Photodecomposition quantum yields, Φ_{Ph}, were measured by irradiating into the main absorption band of solutions with LOCTITE 97034 UV-lamp (λ_{ex} = 366 nm, $I_0(\lambda) \approx 13$ mW cm^{-2}), a green diode laser (λ_{ex} = 532 nm, $I_0(\lambda) \approx 98$ mW cm^{-2}), or a red diode laser (λ_{ex} = 650 nm, $I_0(\lambda) \approx 62$ mW cm^{-2}). Spectra were recorded at incremental time intervals, and the data was utilized in Equation (3.

Two-photon absorption spectra were collected through an open aperture z-scan setup (previously detailed[14]) using solutions (10^{-2} M) in 1 mm cuvette moved through the focal point of the output beam of a OPA pumped by a 1 kHz, ~100 fs Coherent Inc. Legend Elite, in turn seeded by a Coherent Inc. Mira Ti-sapphire laser.[61]

Quantum Chemical Calculations

Taking the output from the GaussView5 program, structures were optimized to the B3LYP/D95* level with the GAUSSIAN09 software package.[67] TD-DFT calculations utilized these optimized conformations, and initially the B3LYP method. The alkoxy and alkyl chains in the *para*-position of phenyl and 9-position of fluorene were shortened to methoxy and methyl groups, respectively, due to the minimal impact these groups have on the results of the calculations.[69]

Results and discussion

Initial Synthesis and Characterization

Through the route shown in Scheme 4, compound **5** was synthesized. ^{1}H and ^{13}C NMR spectroscopy and high resolution mass spectrometry were used to confirm the generation and structure of the compound.

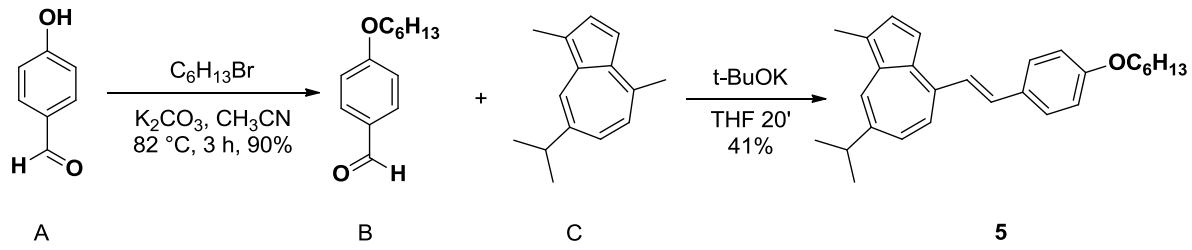

Scheme 4: Synthesis method used to reach guaiazulene derivative **5**.

The absorption spectrum of **5** (Figure 31) shows very little in the visible region (400-800 nm), just the weak $S_0 \rightarrow S_1$ transition of the azulene at ~650 nm. At shorter wavelength, there is much stronger absorbance for the $S_0 \rightarrow S_2$ transition. As expected of an azulene derivative, no emission was observed through excitation at ~650 nm, though nothing was seen for the shorter band either. A summary of the photophysical properties measured for this compound are listed in Table 9.

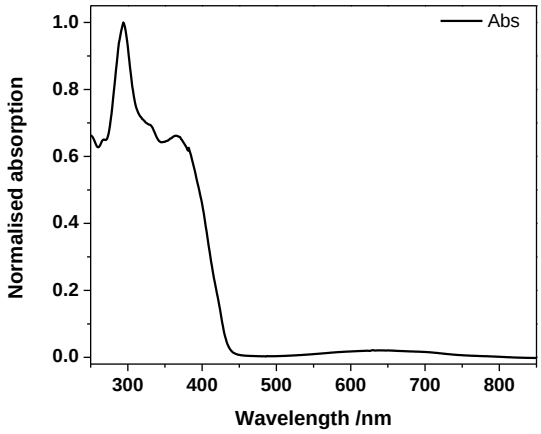

Figure 31: Absorption spectrum of **5** in DCM.

Table 9: Photophysical parameters measured for **5** and **5H** in DCM and 10% TFA/DCM, respectively.

	$\lambda_{max}^{abs\ a}$ /nm	$\lambda_{max}^{em\ a}$ /nm	$\Delta\lambda^{b}$ /nm	ε^{c} /10^3 M^{-1} cm^{-1}	$\Phi_f{}^{d}$	τ^{e} /ns	Φ_{Ph} /10^{-6}
5	294	-[f]	-[f]	29.3	-[f]	-[f]	1000
5H	512	619	93	25.1	0.11	0.87	1.5

[a] Absorption and emission maxima ±1 nm; [b] Stokes shift ±2 nm; [c] extinction coefficients ±5%; [d] fluorescence quantum yields ±10%; [e] fluorescence lifetimes ±10%; [f] not determined.

Dissolution of the compound in a 10% TFA/DCM mixture resulted in a drastic color change from blue to red (Table 9). The absorption spectrum of this protonated species (Figure 32) bears little resemblance to the neutral form: a new peak at 512 nm predominates, attributable to the azulenium cation.[79] Through exciting into this band, a weak fluorescence signal was measured at circa 620 nm. Given the use of a binary solvent system, the refractive index term in Equation

(1) was determined using the Lorentz-Lorenz equation (12), where n_x is the refractive index of solvent x, and ϕ_x is the proportion of solvent x in the mixture.[86]

$$\frac{n_{1,2}^2 - 1}{n_{1,2}^2 + 2} = \phi_1 \frac{n_1^2 - 1}{n_1^2 + 2} + \phi_2 \frac{n_2^2 - 1}{n_2^2 + 2} \quad \textbf{(12)}$$

Using this band, excitation anisotropy was measured for the protonated species. The plateau of this trace through the main absorption band indicates that this is a single electronic transition.

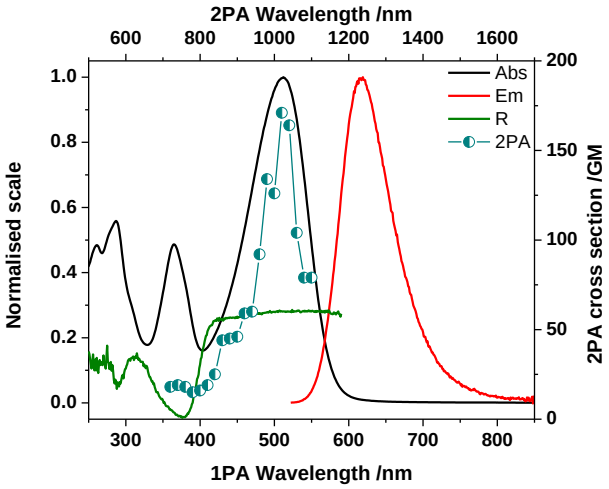

Figure 32: Absorption (black), emission (red), and 2PA spectra (turquoise points) for **5H** in 10% TFA/DCM, and excitation anisotropy (dark green) in acidified silicone oil.

The two-photon absorption spectrum recorded for **5H** includes a respectable peak of ~170 GM at 1020 nm. This overlay with the linear absorption spectrum is not unexpected given the unsymmetrical design of the molecule.

The quantum yields of photodecomposition measured for **5** and **5H** show significant disparity, separated by three orders of magnitude. Though a value is not explicitly stated, the photostability of guaiazulene has been investigated before; the sample was seen to last for a longer period of time than **5** at an equivalent or greater irradiance but no quantitative value was reported.[87] It is possible that change of the solvent from methanol to DCM is responsible for the discrepancy, as a C–Cl bond can be broken using with UV light,[88] leading to additional damage to the compound in solution. In the case of **5H**, longer wavelength light was used, therefore avoiding the degradation of the solvent, and realizing a value similar to those of other fluorescent dyes that have been previously reported.[71]

Examination of the optimized structures for **5** and **5H** reveals that the neutral form does not exhibit a planar conformation (Figure 33a), instead exhibiting a distinct dihedral angle, φ, between the guaiazulene moiety and the vinyl bond (φ = 37.6°). When the 3-position of the guaiazulene is protonated, this twist disappears (φ = 1.12°, Figure 33b), possibly due to the cavity between the two

hydrogen atoms, though the distance between C3 of the guaiazulene and the hydrogen of the second vinyl carbon is 2.4 Å (twice that of an aliphatic C–H bond).

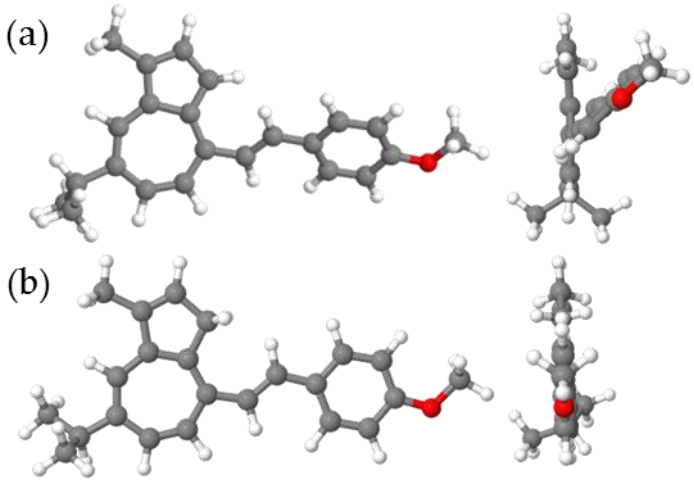

Figure 33: Optimized structures for **5** (a) and **5H** (b).

The ground state stationary dipole for the two forms is consistent (1.90 D and 2.20 D for **5** and **5H**, respectively) despite the present of a positive charge on the protonated form, though the dipole now focuses toward the protonated cyclopentene ring rather than the anethole moiety.

Examination of the absorption spectra generated through the TD-DFT calculations shows that the weak intensity band of the $S_0 \rightarrow S_1$ transition is evident, though the bands at shorter wavelength appear to more resolved than seen experimentally (Figure 34a). In the case of **5H** (Figure 34b), the band

centered at ~600 nm is anticipated by the calculation, however the short wavelength bands are less well aligned.

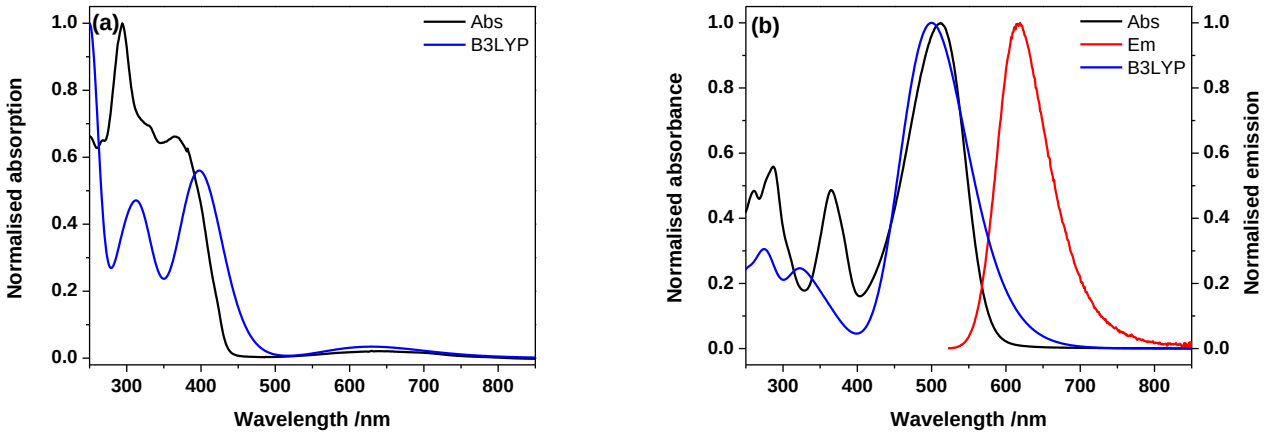

Figure 34: Calculated absorption spectra (blue) overlaid with experimental absorption (black) and emission (red)spectra for **5** (a) and **5H** (b).

Given that the calculated results are somewhat consistent with the experimental data, it does not seem unreasonable to use this methodology to predict the optical properties of further compounds.

Design of a Longer Chromophore

Using compound **5** as a starting point, a series of guaiazulene derivatives were designed with increasing length of their conjugated systems (Figure 35), as well

as the inclusion and varied position of a thiophene ring. Thiophene is seen to be an isostere of benzene, and its use in place of a phenyl ring has been shown to result in a bathochromic shift of the linear absorption spectrum.[89, 90] The length of conjugation is also known to shift the absorption spectrum, but it can also lead to increased two-photon absorption cross sections.[64, 91] Given the ease of transforming the neutral form of a guaiazulene derivative to its conjugate acid, the eleven structures were also investigated with the 3-position of guaiazulene protonated.

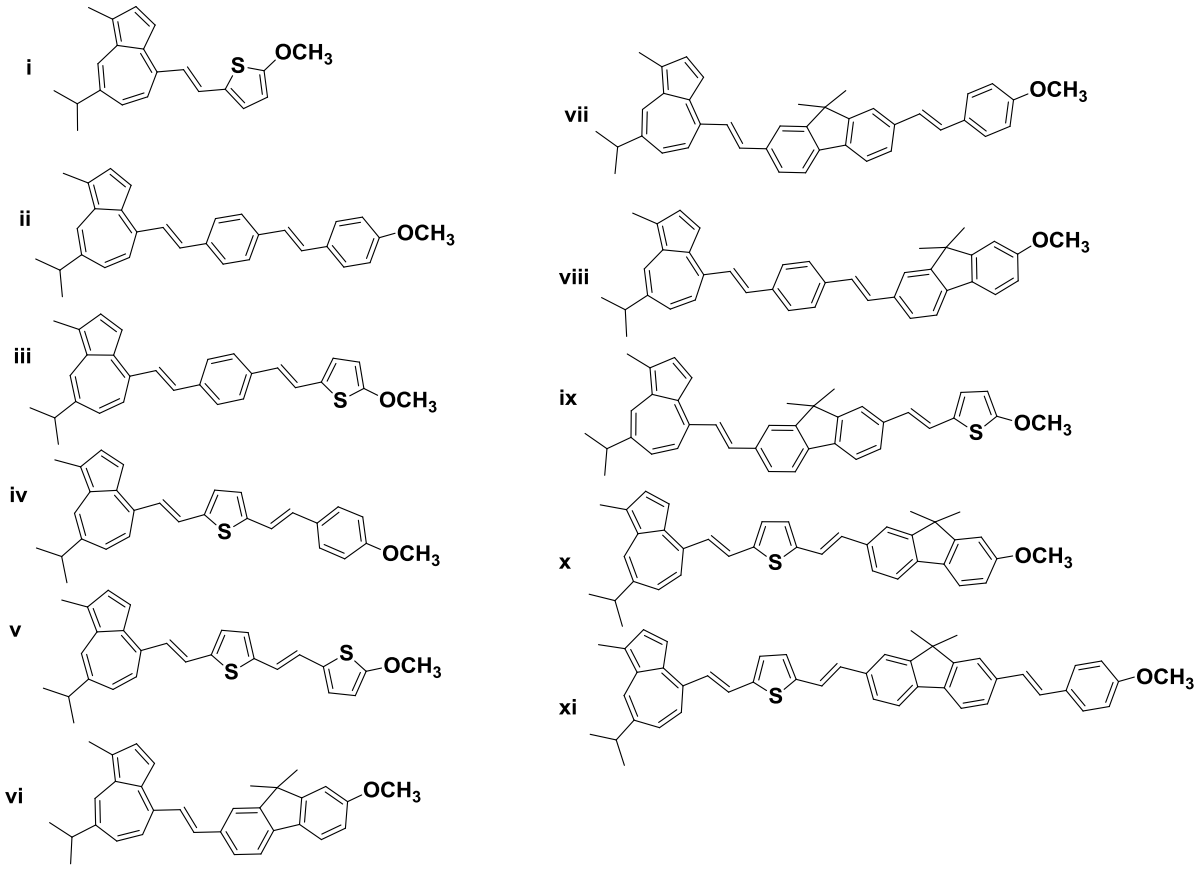

Figure 35: Compounds designed using **5** as a basis.

Analysis of the results from the TD-DFT calculations (Table 10) reveals that the varying length of the chromophore system has little effect on the ground state dipole of the neutral form. However, the protonated forms of the longer systems (vi – xi) show a marked increase on their neutral counterparts, ranging from approximately 3 to 7-fold increases. There is also a noticeable trend in the dihedral angles observed for the optimized structures: the structures with a thiophene ring next to the guaiazulene system (i, iv, v, x, and xi) do not exhibit a

change in dihedral between these systems upon protonation, instead both forms are planar. Conversely, structures with either a phenyl ring or fluorene moiety adjacent to the guaiazulene undergo a ~ 25° rotation to relax the dihedral after being protonated.

The calculation results also show the same bathochromic shift seen for compound **5**, from the weak $S_0 \rightarrow S_1$ band of the azulene at circa 650 nm, and stronger $S_0 \rightarrow S_2$ transition at circa 500 nm, to absorption bands that fall well into the NIR region (Figure 36), behavior that shown for other protonated azulene derivatives.[92]

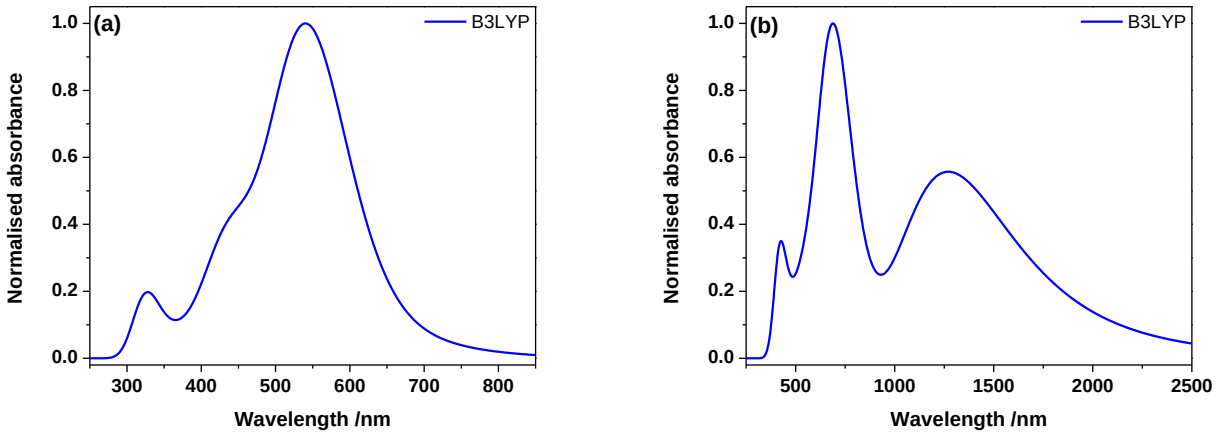

Figure 36: Calculated absorption spectra for **xi** (a) and **xiH** (b) using the B3LYP method.

Table 10: Data collected from TD-DFT calculations on the series of compounds shown in Figure 35.

Cmpd	Dipole /D	Dihedral angle	First transition /nm	λ_{max}^{abs} /nm	Dipole /D	Dihedral angle	First transition /nm	λ_{max}^{abs} /nm
		Neutral form				**Protonated form**		
i	1.62	0.639	639	418	1.39	0.024	527	483
ii	3.13	23.0	650	459	8.34	5.05	753	738
iii	3.11	19.5	653	485	6.56	3.56	758	732
iv	3.14	0.074	677	493	6.13	0.040	683	668
v	4.32	0.001	679	510	4.24	0.017	688	668
vi	2.45	22.7	637	437	8.48	0.004	676	657
vii	3.68	24.1	644	476	15.6	0.000	1009	999
viii	3.02	18.8	657	487	16.7	0.016	966	949
ix	2.59	37.0	647	405	13.0	0.011	1048	1041
x	3.59	0.553	682	519	13.9	0.011	847	842
xi	3.15	0.050	686	540	23.0	0.004	1273	688

To confirm the validity of these results, as well as probe further into the photophysical properties of these extended guaiazulene derivatives, structure **xi** was synthesized and characterized.

Further Synthesis and Characterization

Compound **6** was synthesized as shown in Scheme 5, and ^{1}H and ^{13}C NMR spectroscopy and high resolution mass spectrometry were used to confirm the generation and its structure.

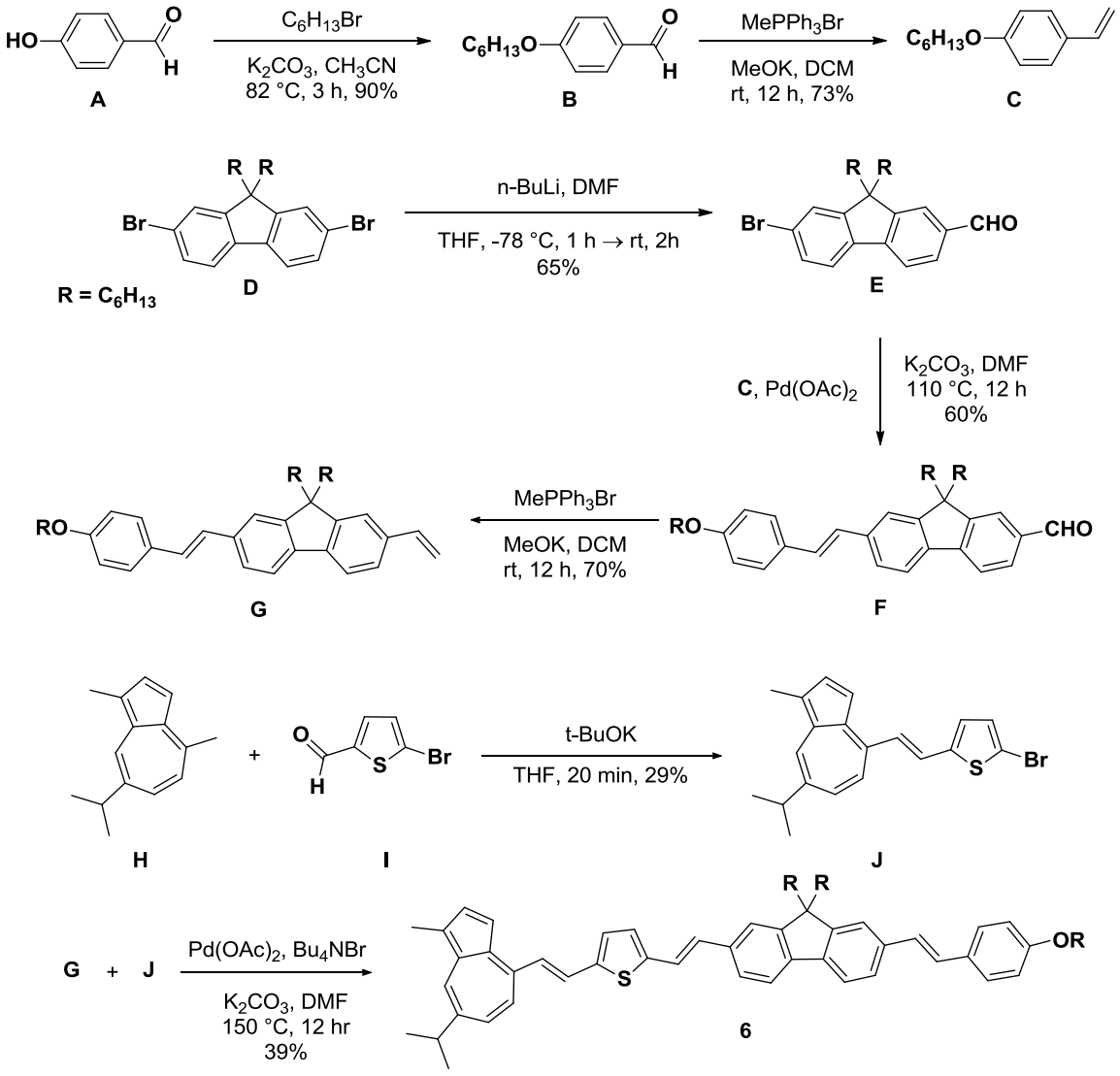

Scheme 5: Synthetic scheme for compound **6**.

The one-photon absorption spectrum of **6** (Figure 37a) shows a 100 nm hypsochromic shift compared to the calculated spectrum, and as such does not conceal the S_0 → S_1 transition at ~ 650 nm. In the case of **6H**, a reasonable agreement is seen between the long wavelength band of the experiment data and

the short band of the calculated spectrum (Figure 37b). However, further probing into the band centered at ~1250 nm using a suitable instrument revealed no evidence of absorption at this wavelength.

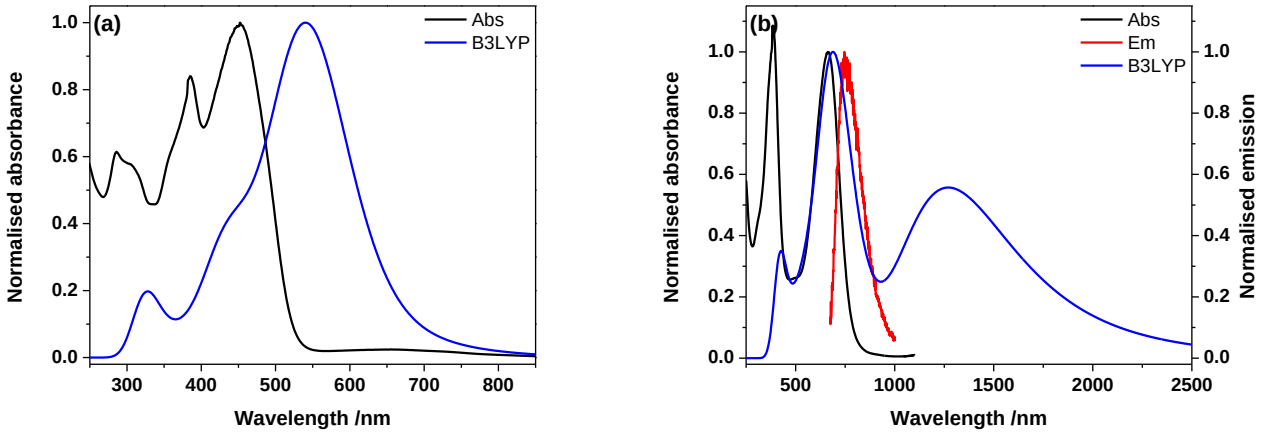

Figure 37: Absorption (black) and emission (red) spectra recorded for **6** in DCM (a) and **6H** in 10% TFA/DCM overlaid with their respective calculated absorption spectra (blue).

Excitation of **6H** at 664 nm results in a fluorescence band centered at 764 nm (Figure 37b), though the quantum yield of this emission is low (Table 11). It can also be noted that the combination of lengthening the chromophore and including a thiophene ring seems to have had a detrimental effect on the extinction coefficients for **6** and **6H**, at roughly half of those for **5** and **5H**. This is counterintuitive as the addition of a thiophene ring has been noted to increase

this value.[93, 94] However, increasing length of the conjugated system has also been shown to decrease extinction coefficient.[64]

Table 11: Photophysical parameters measured for **6** and **6H** in DCM and 10% TFA/DCM, respectively.

	λ_{max}^{abs} [a] /nm	λ_{max}^{em} [a] /nm	$\Delta\lambda$ [b] /nm	ε [c] /10^3 M^{-1} cm^{-1}	Φ_f [d]	τ [e] /ns	Φ_{Ph} /10^{-6}
6	448	- [f]	- [f]	16.1	- [f]	- [f]	- [f]
6H	385, 664	764	100	18.2, 16.9	0.01	1.52	13

[a] Absorption and emission maxima ±1 nm; [b] Stokes shift ±2 nm; [c] extinction coefficients ±5%; [d] fluorescence quantum yields ±10%; [e] fluorescence lifetimes ±10%; [f] not determined.

The increase in the photodecomposition quantum yield of **6H** is nominal, though the compound was noted to have poor stability in solution over time, attributed to the combination of the thiophene, and the acidic solution.

Similar to that of **5H**, the excitation anisotropy of **6H** plateaus within the long wavelength absorption band, in accordance with a sole transition. This plateau also suggests that the absorption and emission are collinear, given its value of 0.4.[9] The two-photon absorption spectrum of **6H** recorded in 10% TFA/DCM (Figure 38) initially shows a reasonable alignment to the linear absorption spectrum, though appears erratic beyond 1300 nm.

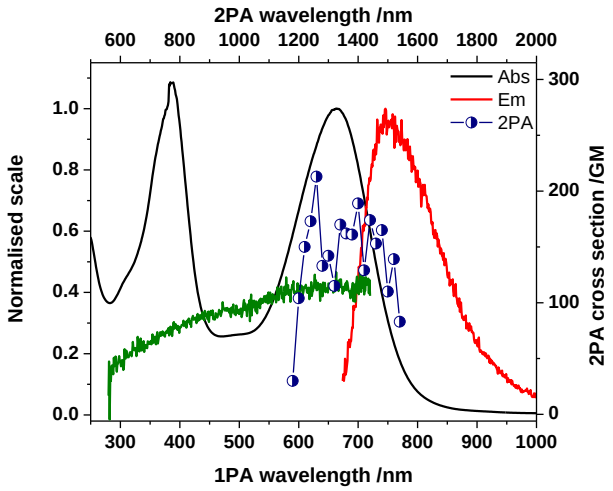

Figure 38: Absorption (black), emission (red), and 2PA spectra (dark blue points) for **6H** in 10% TFA/DCM, and excitation anisotropy trace (dark green) in acidified silicone oil.

In an effort to resolve the difference observed between the experimental results and those of the B3LYP TD-DFT calculation, a series of additional methods were implemented. These methods include differing proportions of Hartree-Fock calculations. Such *ab intio* methods yield results that are less erratic than the semiempirical methods, though at the cost of time.[62] Hybrid functions, including B3LYP (20% Hartree-Fock), have been developed to bridge this gap, where the ratios can be adjusted. With respect to spectroscopic data, increasing the *ab intio* portion blue shifts, or decreases, the wavelength reported for the first (longest wavelength) transition. Figure 39a shows the height of this process, where the one-photon absorption calculated through the M06-HF (100% Hartree-

Fock) method shows acceptable correlation to the experimental, and the two-photon absorption is to the same order of magnitude, with the same disparity as the one-photon absorption (Figure 39b).

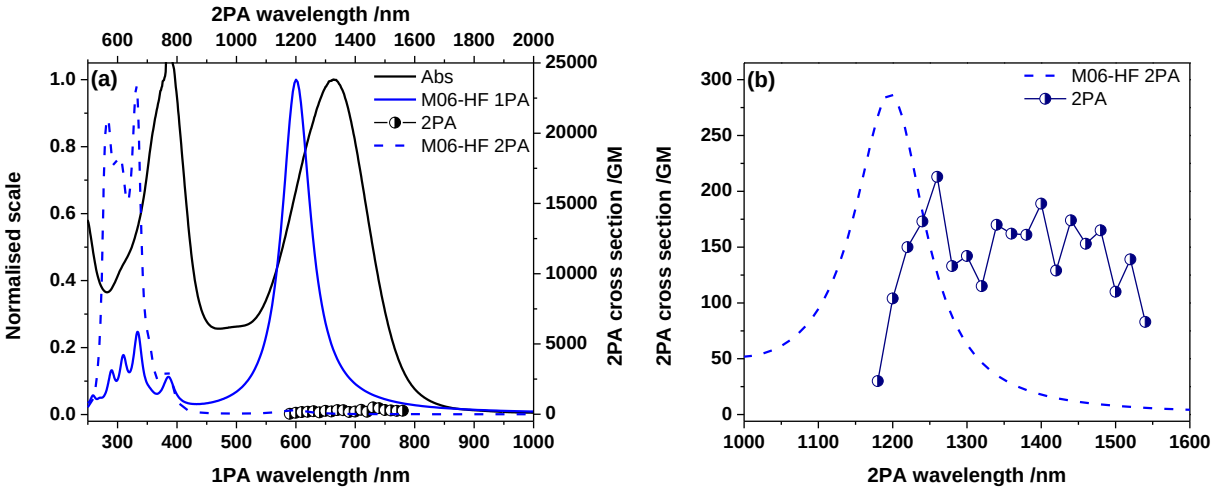

Figure 39: (a) Experimental (black) and M06-HF calculated one-photon absorption (solid blue), and experimental (dark blue points) and M06-HF calculated two-photon absorption (dashed blue); (b) an enlargement of 1000-1600 nm region of the 2PA spectrum.

Conclusions

The compounds synthesized show distinct halochromic behavior, and could be developed into a switchable optoelectronic system. Although it was not possible to provide definite predictions for the compounds investigated computationally, the use of quantum chemical calculations to consider the

properties of designed, yet unsynthesized, compounds is a noteworthy course of action for chemists in this modern, increasingly eco-friendly world.

Future work

Through the synthesis, and subsequent characterization of one of the intermediary length structures from Figure 35, it is intended to investigate to see whether any discernible trend can be determined, otherwise unseen from just these two compounds.

V: CONCLUSIONS

The development of novel two-photon absorbing materials is an area of active research. This work has examined several such materials. A novel fluorene-based donor-acceptor β-diketonate ligand was characterized, and capable of efficient sensitization of a europium center via one and two-photon excitation. Anomalous two-photon data was examined using DFT calculations and explained for a difluoroboron bis-β-diketonate and a Janus dione derivative, both of which display symmetrical structures. A series of guaiazulene derivatives were designed and had photophysical properties predicted for them, which were then tested after the synthesis of one.

Given the different approaches used to reach conclusions, this work supports the notion of combining experimental and computational results in the analysis of compounds from the outset to not only understand photophysical behavior but, perhaps even more significantly, to predict it.

APPENDIX A: CARTESIAN COORDINATES FOR OPTIMIZED STRUCTURES

Optimized geometry for compound **3** obtained using the B3LYP method and D95* basis set.

C	-1.03756	7.21186	-0.23931
C	-1.03547	8.62611	-0.23217
C	0.19149	9.29476	-0.09012
H	-1.97589	9.15476	-0.33249
C	1.27897	7.13134	0.00124
C	1.37098	8.54224	0.03316
H	0.22768	10.37963	-0.07534
H	2.3442	9.00425	0.14877
N	0.09767	6.47757	-0.12921
C	2.51079	6.30953	0.10978
C	2.50892	4.92166	-0.02115
O	3.62749	7.00276	0.3271
C	3.734	4.21163	0.06596
H	1.56698	4.4277	-0.19597
B	4.99505	6.3739	0.51735
C	3.87242	2.76479	-0.08937
O	4.86144	4.87967	0.29947
F	5.87482	6.89776	-0.44687
F	5.42166	6.60212	1.84093
C	5.1548	2.17352	0.09736
C	2.76385	1.94145	-0.43133
C	5.30566	0.80081	-0.0481
H	5.98634	2.82127	0.35434
C	2.91652	0.55864	-0.58405
H	1.78528	2.38372	-0.58974
C	4.19018	-0.01623	-0.3895
H	2.06168	-0.05652	-0.85144
C	4.63842	-1.40476	-0.46268
C	6.03143	-1.45273	-0.17356
C	3.92703	-2.59017	-0.72773
C	6.69486	-2.67852	-0.11235
C	4.59947	-3.81849	-0.6952
H	2.86611	-2.56531	-0.9644
C	5.98465	-3.87995	-0.37954
H	7.74432	-2.73319	0.15419

H	4.06412	-4.73698	-0.91264
N	6.65416	-5.13792	-0.33289
C	8.02874	-5.24752	-0.74469
C	5.96699	-6.31526	0.12635
C	8.94571	-5.99875	0.02541
C	8.47455	-4.61782	-1.92959
C	6.12092	-7.54266	-0.55805
C	5.1419	-6.26378	1.27377
C	10.28406	-6.1189	-0.38727
H	8.60904	-6.48228	0.93788
C	9.81753	-4.73064	-2.32878
H	7.77077	-4.05148	-2.53304
C	5.46275	-8.69655	-0.09855
H	6.75093	-7.58806	-1.44163
C	4.4768	-7.41864	1.71997
H	5.02879	-5.3268	1.81153
C	10.73019	-5.48334	-1.56303
H	10.97911	-6.69947	0.21466
H	10.14613	-4.24353	-3.24381
C	4.63401	-8.64271	1.03964
H	5.59017	-9.63375	-0.63515
H	3.84795	-7.36479	2.60556
H	11.76673	-5.57426	-1.87702
H	4.12368	-9.53588	1.39055
C	-2.32166	6.47696	-0.36416
C	-2.40986	5.08849	-0.27881
O	-3.39243	7.24904	-0.5447
C	-3.68092	4.46409	-0.36509
H	-1.5006	4.52896	-0.13068
B	-4.79794	6.71582	-0.75038
C	-3.91416	3.02625	-0.24626
O	-4.76469	5.21267	-0.55824
F	-5.64535	7.28037	0.21913
F	-5.20206	6.99433	-2.07195
C	-5.24076	2.52982	-0.40151
C	-2.85356	2.11834	0.0263
C	-5.48148	1.16772	-0.28528
H	-6.03474	3.24007	-0.60726

C	-3.0953	0.74456	0.1431
H	-1.84106	2.48723	0.15666
C	-4.41247	0.26442	-0.01301
C	-6.8127	0.41548	-0.40768
H	-2.27507	0.06465	0.35681
C	-4.95517	-1.09088	0.0562
C	-6.35694	-1.03	-0.16897
C	-4.33411	-2.33179	0.29472
C	-7.13204	-2.18768	-0.16456
C	-5.11046	-3.49771	0.30933
H	-3.26516	-2.39743	0.48239
C	-6.51382	-3.44436	0.07716
H	-8.20071	-2.14411	-0.34922
H	-4.64388	-4.45664	0.50931
N	-7.28795	-4.64013	0.09471
C	-8.65187	-4.6215	0.55519
C	-6.72552	-5.88457	-0.35873
C	-9.65682	-5.29989	-0.17096
C	-8.99862	-3.93964	1.74426
C	-6.94621	-7.07304	0.374
C	-5.96185	-5.93799	-1.54775
C	-10.9854	-5.29675	0.28841
H	-9.39494	-5.82377	-1.08567
C	-10.3314	-3.92887	2.19025
H	-8.22797	-3.42781	2.31379
C	-6.41422	-8.29268	-0.07906
H	-7.53017	-7.03687	1.28906
C	-5.42207	-7.15874	-1.98785
H	-5.79897	-5.03067	-2.12241
C	-11.33253	-4.60869	1.46792
H	-11.74921	-5.8221	-0.27994
H	-10.58448	-3.40217	3.10731
C	-5.64622	-8.34398	-1.25924
H	-6.59168	-9.19929	0.49456
H	-4.83885	-7.18568	-2.90528
H	-12.36145	-4.60348	1.81804
H	-5.23304	-9.28789	-1.60515
C	6.58735	-0.0392	0.07017

C	7.56234	0.42838	-1.07545
H	8.42935567	-0.19860651	-1.08392086
C	-7.84871	0.88785	0.66789
H	-8.74052072	0.30238484	0.58540253
C	-7.4621	0.60108	-1.82033
H	-7.70864979	1.63192118	-1.96688943
H	7.85699817	1.44216872	-0.90135522
C	7.27228	0.11048	1.46457
H	7.6056778	1.11922935	1.5917339
H	-8.3510793	0.00908148	-1.88477802
H	-8.08330241	1.91953498	0.50822627
H	8.11030521	-0.55221669	1.52327979
H	6.57042837	-0.13295568	2.23466308
H	7.06289929	0.35916767	-2.01920242
H	-6.77034115	0.28906789	-2.5746629
H	-7.43004454	0.76432402	1.6448038

Optimized geometry for compound **4** obtained using the B3LYP method and D95* basis set.

C	-5.994075	0.647475	-0.060148
C	-7.103706	1.542836	-0.04745
C	-8.398008	1.052967	-0.037506
C	-8.628181	-0.345197	-0.038587
C	-7.547915	-1.24516	-0.050857
C	-6.2439	-0.753131	-0.061945
C	-10.069382	-0.576314	-0.022309
C	-10.728143	0.67397	-0.013033
C	-12.115561	0.748541	0.012803
H	-12.625603	1.708982	0.032709
C	-12.878249	-0.443504	0.020722
C	-12.212089	-1.693409	0.00256
C	-10.818262	-1.763241	-0.012613
H	-6.915141	2.61644	-0.045353
H	-7.719263	-2.32051	-0.050962
H	-12.800782	-2.607179	-0.004398
H	-10.328936	-2.735896	-0.031329
C	-9.719378	1.823116	-0.022548

N	-14.293099	-0.392244	0.040783
C	-15.040365	-1.36527	0.768166
C	-14.634282	-1.76656	2.056018
C	-16.202171	-1.931801	0.208843
C	-15.372637	-2.722867	2.762743
H	-13.742956	-1.328125	2.500065
C	-16.943149	-2.876688	0.928444
H	-16.520657	-1.630345	-0.786918
C	-16.532913	-3.282609	2.207055
H	-15.045433	-3.020756	3.758172
H	-17.838451	-3.306242	0.480542
H	-17.10828	-4.022124	2.761736
C	-14.987996	0.649309	-0.642363
C	-14.614221	1.020513	-1.94891
C	-16.0647	1.312962	-0.022856
C	-15.298571	2.043837	-2.614978
H	-13.790393	0.50513	-2.438557
C	-16.753581	2.32515	-0.701752
H	-16.359376	1.032716	0.986276
C	-16.374076	2.701335	-1.998728
H	-14.998536	2.316757	-3.626009
H	-17.583741	2.829377	-0.208454
H	-16.909055	3.492504	-2.521717
C	-9.848031	2.700429	1.244934
H	-10.826863	3.19564	1.275185
H	-9.738888	2.100337	2.155829
H	-9.076403	3.480625	1.254708
C	-9.878146	2.697695	-1.28867
H	-10.859603	3.188455	-1.298895
H	-9.109943	3.480845	-1.316349
H	-9.785747	2.096198	-2.20057
C	-4.678662	1.247787	-0.068492
H	-4.692797	2.341805	-0.067427
H	-5.39955	-1.434676	-0.071405
C	1.313801	0.419354	-0.080054
C	0.99461	-0.95324	-0.080399
C	-0.326668	-1.410208	-0.080799
C	-1.31368	-0.420163	-0.080215

C	-0.994482	0.952431	-0.08009
C	0.326812	1.409398	-0.080319
C	2.80603	0.60212	-0.078175
C	3.394364	-0.764169	-0.075613
C	2.26495	-1.747409	-0.078696
H	-0.571625	-2.469723	-0.080814
H	0.571747	2.468917	-0.080004
C	-2.264848	1.746604	-0.078186
C	-2.80583	-0.602912	-0.078305
C	-3.394229	0.76331	-0.075376
O	-2.345969	2.969379	-0.078278
O	-3.357233	-1.70137	-0.079331
O	3.357369	1.700646	-0.078618
O	2.346078	-2.97019	-0.079147
C	5.994138	-0.648267	-0.060124
C	7.103895	-1.54345	-0.04726
C	8.398122	-1.053381	-0.03715
C	8.62807	0.344819	-0.038329
C	7.547655	1.244626	-0.050764
C	6.243738	0.752372	-0.061926
C	10.069227	0.576176	-0.022084
C	10.728191	-0.674002	-0.012744
C	12.115617	-0.748358	0.01299
H	12.625805	-1.708722	0.032842
C	12.878128	0.443806	0.020832
C	12.211765	1.693608	0.002731
C	10.817926	1.76322	-0.012401
H	6.915464	-2.617081	-0.045257
H	7.718848	2.319999	-0.050992
H	12.800317	2.607468	-0.004196
H	10.328448	2.735797	-0.031151
C	9.719612	-1.82331	-0.021981
N	14.292978	0.39276	0.040753
C	15.040148	1.365998	0.767975
C	14.634237	1.767139	2.055921
C	16.201638	1.932885	0.208373
C	15.372463	2.723666	2.762489
H	13.743143	1.328419	2.500155

C	16.9425	2.877991	0.927812
H	16.519979	1.631522	-0.787462
C	16.532436	3.283765	2.206524
H	15.04541	3.021451	3.757996
H	17.837566	3.307825	0.479709
H	17.107704	4.023451	2.761078
C	14.988004	-0.648688	-0.64241
C	14.614134	-1.020073	-1.948877
C	16.064942	-1.312057	-0.023
C	15.298618	-2.043295	-2.614962
H	13.790132	-0.504907	-2.438459
C	16.753949	-2.324142	-0.701918
H	16.359688	-1.031692	0.986078
C	16.374352	-2.70051	-1.998814
H	14.998502	-2.316354	-3.625932
H	17.584287	-2.828152	-0.208697
H	16.909433	-3.491598	-2.521818
C	9.848386	-2.700092	1.245851
H	10.827306	-3.195114	1.276303
H	9.739134	-2.09965	2.156503
H	9.076879	-3.480401	1.255928
C	9.878554	-2.698366	-1.287758
H	10.860097	-3.18896	-1.297789
H	9.110502	-3.481675	-1.315149
H	9.786055	-2.097244	-2.199897
C	4.67879	-1.248681	-0.068706
H	4.69295	-2.342697	-0.067846
H	5.399223	1.433698	-0.071414

Optimized geometry for compound **5** obtained using the B3LYP method and D95* basis set.

C	2.940817	-1.770807	-0.110706
C	1.582217	-1.526857	-0.323057
C	0.828915	-0.323015	-0.364104
C	4.021702	-0.898692	0.129937
C	1.377086	0.978516	-0.311431
C	3.917443	0.500464	0.15406

C	2.815841	1.336654	-0.054738
H	3.19707	-2.831647	-0.117859
H	0.984636	-2.43151	-0.442399
H	4.853364	1.031454	0.34014
C	0.699797	2.201433	-0.504719
H	-0.344163	2.316001	-0.766855
C	1.62646	3.256885	-0.36782
H	1.389716	4.313019	-0.48304
C	2.909288	2.752835	-0.077638
C	4.150991	3.580227	0.134569
H	4.586039	3.426407	1.132631
H	4.935097	3.348712	-0.600495
H	3.920075	4.647623	0.040475
C	5.403413	-1.518118	0.362357
H	6.102746	-0.690643	0.541895
C	5.438481	-2.419089	1.615547
H	5.112185	-1.87002	2.507408
H	4.783087	-3.292316	1.502677
H	6.456338	-2.79042	1.794642
C	5.91468	-2.279669	-0.879631
H	5.932059	-1.629317	-1.762875
H	6.932438	-2.65588	-0.710172
H	5.277487	-3.142483	-1.113656
C	-0.626207	-0.549343	-0.489512
H	-0.898748	-1.452038	-1.038009
C	-1.616426	0.172057	0.092126
H	-1.333769	1.013824	0.722605
C	-3.057106	-0.092007	0.015236
C	-3.634443	-1.081363	-0.818909
C	-3.933638	0.677873	0.803249
C	-5.007924	-1.290347	-0.84912
H	-3.001198	-1.690672	-1.460815
C	-5.321133	0.481041	0.786837
H	-3.521942	1.45004	1.453234
C	-5.86779	-0.511413	-0.043761
H	-5.448629	-2.049269	-1.492809
H	-5.954454	1.099651	1.416704
O	-7.198294	-0.797268	-0.149098

C	-8.109506	-0.040135	0.63869
H	-9.10544	-0.425649	0.402054
H	-7.917992	-0.169583	1.714006
H	-8.067402	1.030071	0.388542

Optimized geometry for compound **5H** obtained using the B3LYP method and D95* basis set.

C	-2.779248	-1.969705	-0.173893
C	-1.440165	-1.6449	-0.130874
C	-0.72679	-0.393132	-0.062014
C	-3.94941	-1.151053	-0.171142
C	-1.404417	0.856118	-0.005908
C	-3.917073	0.232395	-0.1024
C	-2.804443	1.110365	-0.019161
H	-2.975703	-3.04116	-0.230532
H	-0.787445	-2.516578	-0.159689
H	-4.882184	0.731764	-0.11309
C	-0.71071	2.198017	0.084545
H	-0.06063	2.374758	-0.785367
C	-1.831912	3.188683	0.128583
H	-1.675476	4.261902	0.198611
C	-3.033007	2.566515	0.065778
C	-4.385337	3.223562	0.080633
H	-4.951614	3.004275	-0.834359
H	-4.989153	2.886205	0.933546
H	-4.281132	4.310213	0.155314
C	-5.278707	-1.899158	-0.205945
H	-5.11939	-2.791567	-0.826734
C	-5.624808	-2.390728	1.223732
H	-4.826145	-3.007891	1.652687
H	-5.795519	-1.541305	1.897092
H	-6.539949	-2.993541	1.197081
C	-6.452795	-1.116317	-0.815054
H	-6.204863	-0.705981	-1.80174
H	-7.309816	-1.787803	-0.93917
H	-6.785453	-0.293924	-0.168766
C	0.71227	-0.584165	-0.052793

H	0.999545	-1.632445	-0.088546
C	1.756435	0.309442	-0.012303
H	1.561215	1.375063	0.020943
C	3.162964	-0.02433	-0.011768
C	3.670917	-1.35428	-0.051033
C	4.104746	1.032938	0.030078
C	5.03096	-1.600593	-0.048552
H	2.993671	-2.204509	-0.083772
C	5.478856	0.803294	0.033394
H	3.74747	2.062221	0.060738
C	5.956979	-0.524635	-0.006293
H	5.423298	-2.614614	-0.078523
H	6.164045	1.644957	0.066521
O	7.253886	-0.877706	-0.007704
C	8.257771	0.144733	0.034726
H	9.21453	-0.381907	0.025178
H	8.19104	0.799213	-0.844159
H	8.175849	0.739174	0.954044
H	-0.075729	2.266743	0.980309

Optimized geometry for compound **6** obtained using the B3LYP method and D95* basis set.

C	10.759768	-1.796563	-0.0001
C	9.514491	-1.172336	0.000028
C	9.139662	0.199637	-0.000005
C	12.075361	-1.28223	-0.000281
C	10.050423	1.283592	-0.000278
C	12.386399	0.082201	-0.000439
C	11.550927	1.206874	-0.000474
H	10.696325	-2.886132	0.000008
H	8.686803	-1.876698	0.000317
H	13.452649	0.317507	-0.000591
C	9.732499	2.662115	-0.000462
H	8.743769	3.104924	-0.000465
C	10.931116	3.401418	-0.000744
H	10.99312	4.488028	-0.000952
C	12.044572	2.535497	-0.00076

C	13.489009	2.964424	-0.001044
H	14.029925	2.59903	0.883613
H	14.029535	2.599167	-0.885997
H	13.563582	4.05798	-0.000975
C	13.232729	-2.285352	-0.000244
H	14.16428	-1.703757	-0.00063
C	13.246533	-3.159681	1.272192
H	13.280119	-2.540882	2.177347
H	12.353315	-3.794741	1.335204
H	14.123289	-3.820927	1.275721
C	13.246046	-3.160529	-1.272077
H	13.27925	-2.542348	-2.177672
H	14.122839	-3.821725	-1.275496
H	12.352854	-3.795697	-1.334333
C	7.708353	0.529816	0.000304
C	6.652496	-0.331768	-0.000306
H	6.828366	-1.406404	-0.001178
C	5.25903	0.062691	0.000016
C	4.668459	1.326017	0.000669
S	4.014674	-1.168803	-0.000479
C	3.255541	1.295337	0.000817
H	5.245254	2.247027	0.001029
C	2.720974	0.006682	0.00022
H	2.638351	2.189764	0.001316
H	7.470646	1.588563	0.001022
C	1.343532	-0.444548	0.00016
C	0.250413	0.366615	0.00075
H	0.415188	1.44531	0.001217
H	1.199751	-1.524976	-0.000358
C	-1.152852	-0.043452	0.000778
C	-1.565836	-1.400225	0.000881
C	-2.150615	0.964093	0.000727
C	-2.916576	-1.749328	0.000862
H	-0.819322	-2.191759	0.001028
C	-3.497726	0.622171	0.000704
H	-1.842951	2.01046	0.000687
C	-3.888988	-0.735223	0.00075
H	-3.206266	-2.799363	0.000966

C	-4.720643	1.541002	0.000621
C	-5.351213	-0.799156	0.000673
C	-5.858374	0.518394	0.000572
C	-6.232917	-1.892671	0.000698
C	-7.230539	0.743445	0.000437
C	-7.608974	-1.659948	0.000563
H	-5.854908	-2.914363	0.000873
C	-8.13836	-0.344485	0.000363
H	-7.625691	1.759896	0.000366
H	-8.285574	-2.511943	0.000694
C	-4.759386	2.427267	1.267629
H	-3.90241	3.112862	1.28734
H	-5.674709	3.032544	1.288664
H	-4.731403	1.817611	2.178179
C	-4.759267	2.427289	-1.266345
H	-3.902287	3.112886	-1.28599
H	-4.731214	1.817673	-2.176924
H	-5.674581	3.03258	-1.287459
C	-9.575913	-0.055358	0.000163
C	-10.591654	-0.954354	-0.000336
H	-10.344838	-2.016958	-0.000652
C	-12.029963	-0.668343	-0.000567
C	-12.57639	0.631774	-0.000348
C	-12.942073	-1.74997	-0.001022
C	-13.957574	0.851981	-0.000541
H	-11.918357	1.49876	-0.000034
C	-14.320358	-1.550129	-0.001203
H	-12.55694	-2.76984	-0.001226
C	-14.843533	-0.243013	-0.000968
H	-14.331131	1.872481	-0.000416
H	-15.01284	-2.389615	-0.001565
H	-9.823533	1.007362	0.000339
O	-16.20598	-0.142742	-0.001192
C	-16.781769	1.157717	-0.000506
H	-16.496607	1.727461	-0.897222
H	-17.865415	1.008049	-0.000338
H	-16.496217	1.726679	0.896608

Optimized geometry for compound **6H** obtained using the B3LYP method and D95* basis set.

C	-10.730687	-1.773985	-0.000069
C	-9.482878	-1.197007	-0.000137
C	-9.051223	0.178786	-0.000093
C	-12.046582	-1.197593	0.000077
C	-9.974808	1.267703	-0.000036
C	-12.300818	0.159336	0.000133
C	-11.384875	1.25364	0.000056
H	-10.714482	-2.863073	-0.000127
H	-8.675786	-1.924735	-0.000246
H	-13.351673	0.445832	0.000238
C	-9.530996	2.716814	-0.000048
H	-8.916546	2.954616	-0.882087
C	-10.817764	3.485184	0.000016
H	-10.866016	4.570943	0.000031
C	-11.881824	2.645233	0.000077
C	-13.334133	3.034193	0.000165
H	-13.855299	2.646155	-0.885285
H	-13.85519	2.646193	0.885695
H	-13.439884	4.123445	0.000147
C	-13.226793	-2.164159	0.00017
H	-14.141995	-1.559231	0.000286
C	-13.251041	-3.035261	-1.275799
H	-13.266574	-2.41944	-2.183074
H	-12.382489	-3.703433	-1.333839
H	-14.148999	-3.664542	-1.277056
C	-13.250776	-3.035353	1.276082
H	-13.266052	-2.419603	2.183409
H	-14.148763	-3.664594	1.277524
H	-12.382243	-3.70357	1.333849
C	-7.64989	0.479123	-0.000111
C	-6.594453	-0.422592	-0.000099
H	-6.804805	-1.491227	-0.000065
C	-5.220439	-0.077736	-0.000106
C	-4.598019	1.189906	-0.000164
S	-3.98833	-1.33498	-0.00004

C	-3.205625	1.137822	-0.000133
H	-5.15789	2.121253	-0.000221
C	-2.684664	-0.177357	-0.000078
H	-2.572835	2.020218	-0.00018
H	-7.382328	1.530975	-0.000101
C	-1.324643	-0.626047	-0.000042
C	-0.235078	0.210666	-0.000073
H	-0.423917	1.285164	-0.000101
H	-1.168697	-1.703657	-0.000019
C	1.16065	-0.163234	-0.000068
C	1.603052	-1.515883	-0.000082
C	2.136876	0.873285	-0.000049
C	2.956724	-1.832133	-0.000073
H	0.874384	-2.323634	-0.000109
C	3.486207	0.563845	-0.000038
H	1.803576	1.911539	-0.000033
C	3.907226	-0.790735	-0.000049
H	3.273374	-2.873689	-0.000086
C	4.690856	1.505245	0
C	5.360949	-0.826662	-0.000035
C	5.844932	0.502386	-0.00001
C	6.261812	-1.908438	-0.000038
C	7.210972	0.751076	0.000011
C	7.62959	-1.651926	-0.000017
H	5.901567	-2.936264	-0.000052
C	8.137655	-0.323207	0.000001
H	7.59019	1.77306	0.000036
H	8.320701	-2.491405	-0.000013
C	4.713457	2.391441	-1.267879
H	3.847822	3.065929	-1.285622
H	5.619444	3.009576	-1.288298
H	4.694705	1.783126	-2.1795
C	4.713425	2.391348	1.267952
H	3.84779	3.065837	1.285736
H	4.69465	1.782963	2.179527
H	5.619408	3.009486	1.288454
C	9.564759	-0.010896	0.000036
C	10.592258	-0.901743	0.000005

H	10.35476	-1.966354	-0.000045
C	12.022974	-0.605249	0.00002
C	12.557612	0.701399	0.000069
C	12.942508	-1.682341	-0.000009
C	13.934965	0.931898	0.000088
H	11.892605	1.562936	0.000095
C	14.317199	-1.47188	0.00001
H	12.564876	-2.704866	-0.000046
C	14.829917	-0.158523	0.000055
H	14.302535	1.954285	0.000134
H	15.01736	-2.304605	-0.000005
H	9.798913	1.054167	0.000064
O	16.185207	-0.048971	0.000059
C	16.76118	1.254786	0.000115
H	16.474694	1.82102	0.897877
H	17.844049	1.103853	0.000078
H	16.47466	1.821119	-0.897577
H	-8.916457	2.954618	0.881927

APPENDIX B: COPYRIGHT PERMISSIONS

Permission for Figure 1

Adam Woodward

From: Barbara Mattson <barb.mattson@nasa.gov>
Sent: 11 September 2014 13:10
To: Adam Woodward
Subject: Re: Copyright permission

Adam -

If you are referring to one of the first two images on that page, they can be used under NASA's Image Use policy:
http://www.nasa.gov/audience/formedia/features/MP_Photo_Guidelines.html

We only ask that the images be credited to NASA's Imagine the Universe. (All of the small pictures used in the first image are in the public domain.) The third image can also be used under NASA's Image use policy, but should be given the same credit we used.

Best of luck with your dissertation! (Not that there's much luck involved. . .)

Barb Mattson, PhD
Project Lead for Imagine the Universe!

On Sep 11, 2014, at 11:52 AM, adam.woodward@ucf.edu wrote:

To whom it may concern,

I am a chemistry graduate student working in Dr Belfield's research group in the Chemistry Department at the University of Central Florida, and am in the process of putting together my PhD dissertation on linear and nonlinear photophysical characterisations of novel organic compounds. I am writing to request permission to reproduce your diagram of the electromagnetic spectrum (on page below) for inclusion in my introduction chapter.

http://imagine.gsfc.nasa.gov/docs/science/know_l1/emspectrum.html

I would appreciate your consideration.

Regards,

Adam Woodward
4078232899
adam.woodward@ucf.edu

1

Permission for Figure 3

Copyright Clearance Center RightsLink®

Home | Create Account | Help | Live Chat

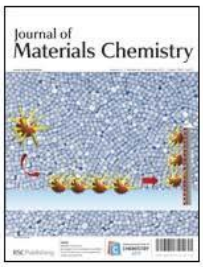

Title: Colour tuning of blue electroluminescence using bipolar carbazole–oxadiazole molecules in single-active-layer organic light emitting devices (OLEDs)

Author: Katharine E. Linton,Alison L. Fisher,Christopher Pearson,Mark A. Fox,Lars-Olof Pålsson,Martin R. Bryce,Michael C. Petty

Publication: Journal of Materials Chemistry

Publisher: Royal Society of Chemistry

Date: May 11, 2012

User ID

Password

Enable Auto Login

LOGIN

Forgot Password/User ID?

If you're a copyright.com user, you can login to RightsLink using your copyright.com credentials. Already **a RightsLink user** or want to learn more?

Quick Price Estimate

The reuse of up to three figures is granted free of charge for academic/educational requestors. Payment is required for the reuse of four or more figures.

I would like to...	reuse in a thesis/dissertation
I am a/an...	academic/educational
The portion I would like to use is...	figures/tables/images
Number of figures/tables/images requested	1
My format is...	print and electronic
My distribution is	
I will be translating...	no
My currency is...	USD - $
Quick Price	Click Quick Price

No content delivery. This service provides permission for reuse only. Once licensed, you may copy and paste the text-only portion of the content according to the terms of your license.

QUICK PRICE CONTINUE

To request permission for a type of use not listed, please contact Royal Society of Chemistry contracts-copyright@rsc.org

Permission for Figure 4

Copyright Clearance Center RightsLink®

Home | Create Account | Help | Live Chat

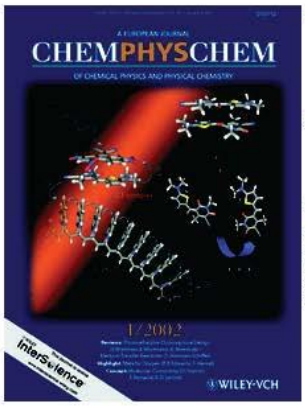

Title: Two-Photon Absorption and Time-Resolved Stimulated Emission Depletion Spectroscopy of a New Fluorenyl Derivative

Author: Kevin D. Belfield,Mykhailo V. Bondar,Alma R. Morales,Xiling Yue,Gheorghe Luchita,Olga V. Przhonska,Olexy D. Kachkovsky

Publication: ChemPhysChem

Publisher: John Wiley and Sons

Date: Aug 7, 2012

User ID

Password

Enable Auto Login

LOGIN

Forgot Password/User ID?

If you're a copyright.com user, you can login to RightsLink using your copyright.com credentials. Already **a RightsLink user** or want to learn more?

Quick Price Estimate

Please review the credit line for the requested figure/table.
If the figure/table you wish to reproduce is credited to a source other than the author of the publication (i.e third party material) you will need to obtain permission from that copyright holder, book or journal before making any use of the material. For the avoidance of doubt – any and all third party content is expressly excluded from this permission.
Otherwise please proceed with your order.

This license allows only minor adaptations as required by the new publication format (with no additions, deletions or modifications to the text that materially alter the meaning of what the author has written). If you wish to make more significant changes to the work please select "I don't see my intended use" and provide full details of your proposed adaptation for review by John Wiley and Sons.

I would like to...	reuse in a dissertation/thesis
Select your currency	USD - $
Requestor Type	University/Academic
Format	Print and electronic
Portion	Figure/table
Number of figures/tables	1
Will you be translating?	No
Quick Price	Click Quick Price

Content Delivery: This service provides permission for reuse only. If you do not have a copy of the content you are using, you may purchase it via Pay-Per-View.

QUICK PRICE CONTINUE

To request permission for a type of use not listed, please contact the publisher directly.

Information regarding permissions for developing countries.

Permission for Figure 7

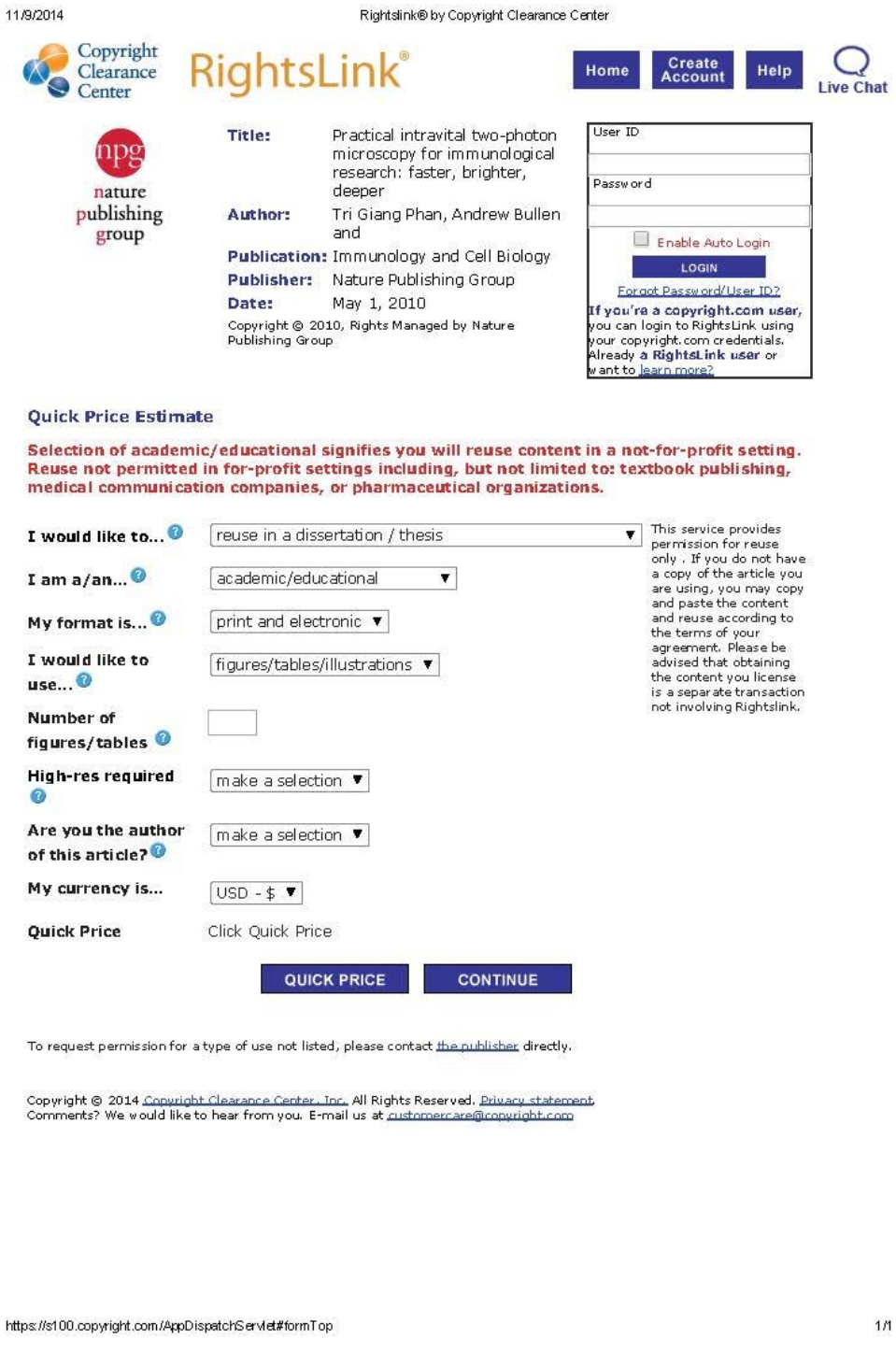

11/9/2014 Rightslink® by Copyright Clearance Center

Copyright Clearance Center RightsLink®

Home | Create Account | Help | Live Chat

nature publishing group

Title: Practical intravital two-photon microscopy for immunological research: faster, brighter, deeper

Author: Tri Giang Phan, Andrew Bullen and

Publication: Immunology and Cell Biology

Publisher: Nature Publishing Group

Date: May 1, 2010

Copyright © 2010, Rights Managed by Nature Publishing Group

User ID

Password

Enable Auto Login

LOGIN

Forgot Password/User ID?

If you're a copyright.com user, you can login to RightsLink using your copyright.com credentials. Already **a RightsLink user** or want to learn more?

Quick Price Estimate

Selection of academic/educational signifies you will reuse content in a not-for-profit setting. Reuse not permitted in for-profit settings including, but not limited to: textbook publishing, medical communication companies, or pharmaceutical organizations.

I would like to... reuse in a dissertation / thesis

I am a/an... academic/educational

My format is... print and electronic

I would like to use... figures/tables/illustrations

Number of figures/tables

High-res required make a selection

Are you the author of this article? make a selection

My currency is... USD - $

Quick Price Click Quick Price

This service provides permission for reuse only . If you do not have a copy of the article you are using, you may copy and paste the content and reuse according to the terms of your agreement. Please be advised that obtaining the content you license is a separate transaction not involving Rightslink.

QUICK PRICE | CONTINUE

To request permission for a type of use not listed, please contact the publisher directly.

Copyright © 2014 Copyright Clearance Center, Inc. All Rights Reserved. Privacy statement.
Comments? We would like to hear from you. E-mail us at customercare@copyright.com

https://s100.copyright.com/AppDispatchServlet#formTop 1/1

Creative Commons Licence for Figure 8

Creative Commons

Creative Commons License Deed

Attribution 4.0 International (CC BY 4.0)

This is a human-readable summary of (and not a substitute for) the license.
Disclaimer

You are free to:

Share — copy and redistribute the material in any medium or format

Adapt — remix, transform, and build upon the material

for any purpose, even commercially.

The licensor cannot revoke these freedoms as long as you follow the license terms.

Under the following terms:

Attribution — You must give appropriate credit, provide a link to the license, and indicate if changes were made. You may do so in any reasonable manner, but not in any way that suggests the licensor endorses you or your use.

No additional restrictions — You may not apply legal terms or technological measures that legally restrict others from doing anything the license permits.

Notices:

You do not have to comply with the license for elements of the material in the public domain or where your use is permitted by an applicable exception or limitation.

No warranties are given. The license may not give you all of the permissions necessary for your intended use. For example, other rights such as publicity, privacy, or moral rights may limit how you use the material.

The applicable mediation rules will be designated in the copyright notice published with the work, or if none then in the request for mediation. Unless otherwise designated in a copyright notice attached to the work, the UNCITRAL Arbitration Rules apply to any arbitration.

More info.

You may also use a license listed as compatible at https://creativecommons.org/compatiblelicenses

More info.

A commercial use is one primarily intended for commercial advantage or monetary compensation.

More info.

Merely changing the format never creates a derivative.

More info.

Permission for Chapter II

Two-photon sensitized visible and near-IR luminescence of lanthanide complexes using a fluorene-based donor–π-acceptor diketonate

A. W. Woodward, A. Frazer, A. R. Morales, J. Yu, A. F. Moore, A. D. Campiglia, E. V. Jucov, T. V. Timofeeva and K. D. Belfield, *Dalton Trans.*, 2014, Advance Article, **DOI:** 10.1039/C4DT01507J

REFERENCES

1. G. G. Stokes, *Philosophical Transactions of the Royal Society of London*, 1852, **142**, 463-562.
2. R. H. Lipson, *Encyclopedia of Applied Spectroscopy: Ultraviolet and Visible Absorption Spectroscopy*, Wiley, 2009.
3. M. Dell'Angela, T. Anniyev, M. Beye, R. Coffee, A. Föhlisch, J. Gladh, T. Katayama, S. Kaya, O. Krupin, J. LaRue, A. Møgelhøj, D. Nordlund, J. K. Nørskov, H. Öberg, H. Ogasawara, H. Öström, L. G. M. Pettersson, W. F. Schlotter, J. A. Sellberg, F. Sorgenfrei, J. J. Turner, M. Wolf, W. Wurth and A. Nilsson, *Science*, 2013, **339**, 1302-1305.
4. V. Voliani, F. Ricci, G. Signore, R. Nifosì, S. Luin and F. Beltram, *Small*, 2011, **7**, 3271-3275.
5. C. H. Townes and A. L. Schawlow, *Microwave Spectroscopy*, Dover Publications, 2013.
6. P. Larkin, *Infrared and Raman Spectroscopy; Principles and Spectral Interpretation*, Elsevier Science, 2011.
7. *Electromagnetic Spectrum - Introduction*, http://imagine.gsfc.nasa.gov/docs/science/know_l1/emspectrum.html, Accessed 11 Sept 2014.
8. K. E. Linton, A. L. Fisher, C. Pearson, M. A. Fox, L.-O. Palsson, M. R. Bryce and M. C. Petty, *Journal of Materials Chemistry*, 2012, **22**, 11816-11825.
9. J. R. Lakowicz, *Principles of Fluorescence Spectroscopy*, Springer, 2007.
10. C. Reichardt, *Solvents and Solvent Effects in Organic Chemistry*, Wiley, 2006.
11. L. Porrès, A. Holland, L.-O. Pålsson, A. Monkman, C. Kemp and A. Beeby, *J Fluoresc*, 2006, **16**, 267-273.
12. J. D. Ingle and S. R. Crouch, *Spectrochemical analysis*, Prentice Hall PTR, 1988.
13. B. Wardle, *Principles and Applications of Photochemistry*, Wiley, 2009.
14. K. D. Belfield, M. V. Bondar, A. R. Morales, X. Yue, G. Luchita, O. V. Przhonska and O. D. Kachkovsky, *ChemPhysChem*, 2012, **13**, 3481-3491.
15. C. C. Corredor, K. D. Belfield, M. V. Bondar, O. V. Przhonska and S. Yao, *Journal of Photochemistry and Photobiology A: Chemistry*, 2006, **184**, 105-112.
16. M. Göppert-Mayer, *Annalen der Physik*, 1931, **401**, 273-294.
17. W. Kaiser and C. G. B. Garrett, *Physical Review Letters*, 1961, **7**, 229-231.
18. R. Menzel, in *Photonics*, Springer Berlin Heidelberg, Editon edn., 2007, pp. 263-358.

19. Z. Li, M. Siklos, N. Pucher, K. Cicha, A. Ajami, W. Husinsky, A. Rosspeintner, E. Vauthey, G. Gescheidt, J. Stampfl and R. Liska, *Journal of Polymer Science Part A: Polymer Chemistry*, 2011, **49**, 3688-3699.
20. C. C. Corredor, Z. L. Huang and K. D. Belfield, *Advanced Materials*, 2006, **18**, 2910-2914.
21. C. O. Yanez, A. R. Morales, X. Yue, T. Urakami, M. Komatsu, T. A. H. Järvinen and K. D. Belfield, *PLoS ONE*, 2013, **8**, e67559.
22. *Photophysics & Photochemistry | Belfield Research Group*, http://chemistry.cos.ucf.edu/belfield/photophysics, Accessed 11 Sept 2014.
23. T. G. Phan and A. Bullen, *Immunol Cell Biol*, 2010, **88**, 438-444.
24. X. Wang, D. M. Nguyen, C. O. Yanez, L. Rodriguez, H.-Y. Ahn, M. V. Bondar and K. D. Belfield, *Journal of the American Chemical Society*, 2010, **132**, 12237-12239.
25. S. Yao and K. D. Belfield, *European Journal of Organic Chemistry*, 2012, **2012**, 3199-3217.
26. J.-C. G. Bunzli, *Chemistry Letters*, 2009, **38**, 104-109.
27. T. Gunnlaugsson and F. Stomeo, *Organic & Biomolecular Chemistry*, 2007, **5**, 1999-2009.
28. J. Hovinen and P. M. Guy, *Bioconjugate Chemistry*, 2008, **20**, 404-421.
29. R. Reyes, M. Cremona, E. E. S. Teotonio, H. F. Brito and O. L. Malta, *Chemical Physics Letters*, 2004, **396**, 54-58.
30. K. Kuriki, Y. Koike and Y. Okamoto, *Chemical Reviews*, 2002, **102**, 2347-2356.
31. J. C. G. Bunzli, S. Comby, A. S. Chauvin and C. D. B. Vandevyver, *J. Rare Earths*, 2007, **25**, 257-274.
32. K. Binnemans, *Rare-Earth β-Diketonates*, K. A. Gschneidner, Jr., Bünzli, Jean-Claude G., and Pecharsky, Vitalij K., ed., *Handbook on the Physics and Chemistry of Rare Earths*, **35**, Elsevier, Amsterdam, 2005.
33. C. Freund, W. Porzio, U. Giovanella, F. Vignali, M. Pasini, S. Destri, A. Mech, S. Di Pietro, L. Di Bari and P. Mineo, *Inorganic Chemistry*, 2011, **50**, 5417-5429.
34. N. M. Shavaleev, R. Scopelliti, F. Gumy and J.-C. G. Bünzli, *Inorganic Chemistry*, 2009, **48**, 6178-6191.
35. A. D'Aléo, A. Picot, A. Beeby, J. A. Gareth Williams, B. Le Guennic, C. Andraud and O. Maury, *Inorganic Chemistry*, 2008, **47**, 10258-10268.
36. L.-M. Fu, X.-F. Wen, X.-C. Ai, Y. Sun, Y.-S. Wu, J.-P. Zhang and Y. Wang, *Angewandte Chemie International Edition*, 2005, **44**, 747-750.

37. A. R. Morales, A. Frazer, A. W. Woodward, H.-Y. Ahn-White, A. Fonari, P. Tongwa, T. Timofeeva and K. D. Belfield, *The Journal of Organic Chemistry*, 2013, **78**, 1014-1025.
38. S. Yao, H.-Y. Ahn, X. Wang, J. Fu, E. W. Van Stryland, D. J. Hagan and K. D. Belfield, *The Journal of Organic Chemistry*, 2010, **75**, 3965-3974.
39. A. F. Moore, F. Barbosa, Jr. and A. D. Campiglia, *Applied spectroscopy*, 2014, **68**, 14-25.
40. K. D. Belfield, M. V. Bondar, A. R. Morales, A. Frazer, I. A. Mikhailov and O. V. Przhonska, *The Journal of Physical Chemistry C*, 2013, **117**, 11941-11952.
41. W. V. Moreshead, O. V. Przhonska, M. V. Bondar, A. D. Kachkovski, I. H. Nayyar, A. E. Masunov, A. W. Woodward and K. D. Belfield, *The Journal of Physical Chemistry C*, 2013, **117**, 23133-23147.
42. C. Xu and W. W. Webb, *J. Opt. Soc. Am. B*, 1996, **13**, 481-491.
43. K. D. Belfield, A. R. Morales, J. M. Hales, D. J. Hagan, E. W. Van Stryland, V. M. Chapela and J. Percino, *Chemistry of Materials*, 2004, **16**, 2267-2273.
44. K. D. Belfield, A. R. Morales, B.-S. Kang, J. M. Hales, D. J. Hagan, E. W. Van Stryland, V. M. Chapela and J. Percino, *Chemistry of Materials*, 2004, **16**, 4634-4641.
45. X. Zhang, Z.-C. Li, C.-F. Lao, D.-C. Zou, F.-Z. Lu, G.-Q. Chen, F.-S. Du and F.-M. Li, *Polymer*, 2006, **47**, 3390-3400.
46. X. Zhang, Z.-C. Li, N. Xu, K.-B. Li, S. Lin, F.-Z. Lu, F.-S. Du and F.-M. Li, *Tetrahedron Letters*, 2006, **47**, 2623-2626.
47. J. E. Rogers, J. E. Slagle, D. G. McLean, R. L. Sutherland, B. Sankaran, R. Kannan, L.-S. Tan and P. A. Fleitz, *The Journal of Physical Chemistry A*, 2004, **108**, 5514-5520.
48. S. I. Klink, G. A. Hebbink, L. Grave, P. G. B. Oude Alink, F. C. J. M. van Veggel and M. H. V. Werts, *The Journal of Physical Chemistry A*, 2002, **106**, 3681-3689.
49. M. Shi, F. Li, T. Yi, D. Zhang, H. Hu and C. Huang, *Inorganic Chemistry*, 2005, **44**, 8929-8936.
50. A. D'Aléo, J. Xu, E. G. Moore, C. J. Jocher and K. N. Raymond, *Inorganic Chemistry*, 2008, **47**, 6109-6111.
51. J. Andres and A.-S. Chauvin, *Physical Chemistry Chemical Physics*, 2013, **15**, 15981-15994.
52. G. A. Hebbink, S. I. Klink, L. Grave, P. G. B. Oude Alink and F. C. J. M. van Veggel, *ChemPhysChem*, 2002, **3**, 1014-1018.

53. S. I. Klink, L. Grave, D. N. Reinhoudt, F. C. J. M. van Veggel, M. H. V. Werts, F. A. J. Geurts and J. W. Hofstraat, *The Journal of Physical Chemistry A*, 2000, **104**, 5457-5468.
54. M. H. V. Werts, R. T. F. Jukes and J. W. Verhoeven, *Physical Chemistry Chemical Physics*, 2002, **4**, 1542-1548.
55. N. S. Makarov, M. Drobizhev and A. Rebane, *Opt. Express*, 2008, **16**, 4029-4047.
56. W. L. Peticolas, *Annual Review of Physical Chemistry*, 1967, **18**, 233-260.
57. P. Atkins and J. De Paula, *Atkins' Physical Chemistry*, Macmillan Higher Education, 2006.
58. C. E. Housecroft and A. G. Sharpe, *Inorganic Chemistry*, 2nd edn., Pearson Prentice Hall, 2005.
59. P. Atkins, *Shriver and Atkins' Inorganic Chemistry*, OUP Oxford, 2010.
60. K. D. Belfield, M. V. Bondar, C. O. Yanez, F. E. Hernandez and O. V. Przhonska, *Journal of Materials Chemistry*, 2009, **19**, 7498-7502.
61. K. D. Belfield, M. V. Bondar, F. E. Hernandez, O. V. Przhonska and S. Yao, *The Journal of Physical Chemistry B*, 2007, **111**, 12723-12729.
62. D. C. Young, *Computational chemistry : a practical guide for applying techniques to real world problems*, Wiley, New York, 2001.
63. A. Loudet and K. Burgess, *Chemical Reviews*, 2007, **107**, 4891-4932.
64. L. A. Padilha, S. Webster, O. V. Przhonska, H. Hu, D. Peceli, T. R. Ensley, M. V. Bondar, A. O. Gerasov, Y. P. Kovtun, M. P. Shandura, A. D. Kachkovski, D. J. Hagan and E. W. V. Stryland, *The Journal of Physical Chemistry A*, 2010, **114**, 6493-6501.
65. P. Krief, J. Y. Becker, A. Ellern, V. Khodorkovsky, O. Neilands and L. Shapiro, *Synthesis*, 2004, **2004**, 2509-2512.
66. R. Gvishi, G. Berkovic, Z. Kotler, P. Krief, L. Shapiro, J. T. Klug, J. Skorka and V. Khodorkovsky, Proceedings of SPIE Vol 5211 Nonlinear Optical Transmission and Multiphoton Processes in Organics, 2003.
67. M. J. Frisch, G. W. Trucks, H. B. Schlegel, G. E. Scuseria, M. A. Robb, J. R. Cheeseman, G. Scalmani, V. Barone, B. Mennucci, G. A. Petersson, H. Nakatsuji, M. Caricato, X. Li, H. P. Hratchian, A. F. Izmaylov, J. Bloino, G. Zheng, J. L. Sonnenberg, M. Hada, M. Ehara, K. Toyota, R. Fukuda, J. Hasegawa, M. Ishida, T. Nakajima, Y. Honda, O. Kitao, H. Nakai, T. Vreven, J. A. Montgomery Jr., J. E. Peralta, F. Ogliaro, M. J. Bearpark, J. Heyd, E. N. Brothers, K. N. Kudin, V. N. Staroverov, R. Kobayashi, J. Normand, K. Raghavachari, A. P. Rendell, J. C. Burant, S. S. Iyengar, J. Tomasi, M. Cossi, N. Rega, N. J. Millam, M. Klene, J. E. Knox, J. B. Cross,

V. Bakken, C. Adamo, J. Jaramillo, R. Gomperts, R. E. Stratmann, O. Yazyev, A. J. Austin, R. Cammi, C. Pomelli, J. W. Ochterski, R. L. Martin, K. Morokuma, V. G. Zakrzewski, G. A. Voth, P. Salvador, J. J. Dannenberg, S. Dapprich, A. D. Daniels, Ö. Farkas, J. B. Foresman, J. V. Ortiz, J. Cioslowski and D. J. Fox, GAUSSIAN 09 REV C.01, 2009, Wallingford, CT, USA

68. I. A. Mikhailov, M. V. Bondar, K. D. Belfield and A. E. Masunov, *The Journal of Physical Chemistry C*, 2009, **113**, 20719-20724.
69. K. D. Belfield, M. V. Bondar, F. E. Hernandez, A. E. Masunov, I. A. Mikhailov, A. R. Morales, O. V. Przhonska and S. Yao, *The Journal of Physical Chemistry C*, 2009, **113**, 4706-4711.
70. K. D. Belfield, C. D. Andrade, C. O. Yanez, M. V. Bondar, F. E. Hernandez and O. V. Przhonska, *The Journal of Physical Chemistry B*, 2010, **114**, 14087-14095.
71. K. D. Belfield, M. V. Bondar, A. R. Morales, L. A. Padilha, O. V. Przhonska and X. Wang, *Chemphyschem*, 2011, **12**, 2755-2762.
72. P. T. Anastas and J. C. Warner, *Green Chemistry: Theory and Practice*, Oxford University Press, 1998.
73. S. Das, A. Nag, K. K. Sadhu, D. Goswami and P. K. Bharadwaj, *Journal of Organometallic Chemistry*, 2007, **692**, 4969-4977.
74. L. Moity, V. Molinier, A. Benazzouz, R. Barone, P. Marion and J.-M. Aubry, *Green Chemistry*, 2014, **16**, 146-160.
75. A. Monti, H. J. M. de Groot and F. Buda, *The Journal of Physical Chemistry C*, 2014, **118**, 15600-15609.
76. C. Collins, M. S. Dyer, A. Demont, P. A. Chater, M. F. Thomas, G. R. Darling, J. B. Claridge and M. J. Rosseinsky, *Chemical Science*, 2014, **5**, 1493-1505.
77. A. D. Harmon, K. H. Weisgraber and U. Weiss, *Experientia*, 1980, **36**, 54-56.
78. N. Fusetani, S. Matsunaga and S. Konosu, *Experientia*, 1981, **37**, 680-681.
79. E. Amir, R. J. Amir, L. M. Campos and C. J. Hawker, *Journal of the American Chemical Society*, 2011, **133**, 10046-10049.
80. F. Wang and Y.-H. Lai, *Macromolecules*, 2003, **36**, 536-538.
81. M. Koch, O. Blacque and K. Venkatesan, *Journal of Materials Chemistry C*, 2013, **1**, 7400-7408.
82. E. Amir, M. Murai, R. J. Amir, J. S. Cowart, M. L. Chabinyc and C. J. Hawker, *Chemical Science*, 2014.
83. X. Wang, J. K.-P. Ng, P. Jia, T. Lin, C. M. Cho, J. Xu, X. Lu and C. He, *Macromolecules*, 2009, **42**, 5534-5544.

84. L. Beverina, J. Fu, A. Leclercq, E. Zojer, P. Pacher, S. Barlow, E. W. Van Stryland, D. J. Hagan, J.-L. Brédas and S. R. Marder, *Journal of the American Chemical Society*, 2005, **127**, 7282-7283.
85. M. Grätzel, *Journal of Photochemistry and Photobiology C: Photochemistry Reviews*, 2003, **4**, 145-153.
86. H. A. Lorentz, *The Theory of Electrons and Its Applications to the Phenomena of Light and Radiant Heat: A Course of Lectures Delivered in Columbia University, New York, in March and April, 1906*, B.G. Teubner, 1909.
87. J. Fiori, R. Gotti, A. Albini and V. Cavrini, *Rapid Communications in Mass Spectrometry*, 2008, **22**, 2698-2706.
88. J. A. Dean and N. A. Lange, *Lange's Handbook of Chemistry*, 15th edn., McGraw-Hill, 1999.
89. S. Rihn, P. Retailleau, N. Bugsaliewicz, A. D. Nicola and R. Ziessel, *Tetrahedron Letters*, 2009, **50**, 7008-7013.
90. X. Zhang, H. Yu and Y. Xiao, *The Journal of Organic Chemistry*, 2011, **77**, 669-673.
91. M. Albota, D. Beljonne, J.-L. Brédas, J. E. Ehrlich, J.-Y. Fu, A. A. Heikal, S. E. Hess, T. Kogej, M. D. Levin, S. R. Marder, D. McCord-Maughon, J. W. Perry, H. Röckel, M. Rumi, G. Subramaniam, W. W. Webb, X.-L. Wu and C. Xu, *Science*, 1998, **281**, 1653-1656.
92. F. Wang, T. T. Lin, C. He, H. Chi, T. Tang and Y.-H. Lai, *Journal of Materials Chemistry*, 2012, **22**, 10448-10451.
93. S. Wang, J. Guo, L. He, H. Wang, J. Zhao and C. Lu, *Synthetic Metals*, 2013, **168**, 1-8.
94. L. Zhao, W. Wang and M.-S. Yuan, *Spectrochimica Acta Part A: Molecular and Biomolecular Spectroscopy*, 2015, **135**, 63-68.